DEPARTMENT OF PHYSICS
UNIVERSITY OF JYVÄSKYLÄ
RESEARCH REPORT No. 12/2018

THEORETICAL PREDICTIONS OF WIMP-NUCLEUS AND NEUTRINO-NUCLEUS SCATTERING IN CONTEXT OF DARK MATTER DIRECT DETECTION

BY
PEKKA PIRINEN

Academic Dissertation
for the Degree of
Doctor of Philosophy

To be presented, by permission of the
Faculty of Mathematics and Natural Sciences
of the University of Jyväskylä,
for public examination in Auditorium FYS1 of the
University of Jyväskylä on December 7, 2018
at 12 o'clock noon

Jyväskylä, Finland
December 2018

ISBN: 978-951-39-7618-7 (Printed version)
ISBN: 978-951-39-7619-4 (Electronic version)
ISSN: 0075-465X

Preface

The work reported in this thesis has been carried our during the years 2015–2018 at the University of Jyväskylä. Financial support from the Magnus Ehrnrooth foundation is gratefully acknowledged.

First and foremost I owe thanks to my supervisor, Jouni Suhonen, for expert guidance and support during the work done for this thesis. I always felt reassured after discussing things over with Jouni, even on the rare occasion that I left the room none the wiser.

Big thanks are in order to John D. Vergados for offering the initial motivation to pursue this research topic. Thanks to Markus Kortelainen, Praveen Srivastava, Frank Avignone III, Anthony Thomas, and Emanuel Ydrefors for collaboration. For work that almost came to be for this thesis, I'd like to thank Jenni Kotila. Thanks to Teocharis Kosmas and Doron Gazit for the expert review and insightful comments and suggestions on the thesis manuscript, and Achim Schwenk for agreeing to be the opponent on the day of the defense.

Here's to good friends! I would not have survived this process if it weren't for your support. I wish to thank all my friends and colleagues at the department of Physics for a wonderful atmosphere to do research. Special thanks to the Holvi collaboration and the associated lunchtime advisory board. The university wind band Puhkupillit also deserves a special mention.

I wish to thank Matias Kangas and Lasse Vuori for countless hours of fighting demons during the early stages of my PhD studies. I owe thanks to Valtteri Lahti for showing me to the shores of the cosmic ocean, Juha Suutari for his ever-motivating presence, and Petja Paakkinen for sharing this journey from the beginning till the very end.

I would like to thank my family for encouragement to pursue my goals. In particular, huge thanks are in order to my wife, Miia, and my son, Reino, for unconditional love and support throughout this adventure.

Jyväskylä, November 2018
Pekka Pirinen

Abstract

The nature of dark matter is at present an open question. Assuming the main component of dark matter consists of weakly interacting massive particles (WIMPs), directly detecting such particle via a scattering process with an atomic nucleus would be a strong probe into properties of dark matter. So far direct detection experiments have not provided a conclusive signal of dark matter. Traditionally the experiments aim to detect a coherent, spin-independent, elastic scattering signal which is enhanced by the square of the nuclear mass number. If the coherent channel is for some reason suppressed for WIMP-nucleus interactions, then spin-dependent interactions become important.

In this thesis we focus on spin-dependent interactions of WIMPs scattering off two possible detector nuclei ^{83}Kr and ^{125}Te. These nuclei are particularly interesting for inelastic scattering due to their very low-lying first excited states. The nuclear structure of the target nuclei was computed within the nuclear shell model. Our analysis shows that, although the 9.4 keV excited state of ^{83}Kr has some kinematical advantages, the obtained elastic and inelastic scattering event rates do not encourage to build a detector based on ^{83}Kr. On the other hand, ^{125}Te appears to possess nuclear structure very sensitive to spin-dependent interactions based on the results presented in this thesis. A detector based on ^{125}Te might open some new possibilities especially for inelastic scattering searches.

With increasing size and sensitivity direct detection experiments will soon become sensitive to coherent scattering of astrophysical neutrinos. This gives rise to the problem commonly referred to as the neutrino floor, which will prevent the experiments probing lower WIMP-nucleon cross sections after the neutrino background becomes visible in the data. In this thesis we present the first calculations of neutrino-nucleus scattering cross sections in a microscopic nuclear framework for most of the stable Xe isotopes. We perform the nuclear structure calculations in the framework of the (proton-neutron) quasiparticle random-phase approximation ((pn)QRPA) for states of even-mass nuclei and in the microscopic quasiparticle-phonon model for states of odd-mass

nuclei. We present results for the total cross sections for neutral-current and charged-current processes as a function of the neutrino energy as well as for the solar ^{8}B neutrino and supernova neutrino and antineutrino profiles.

This thesis consists of five publications and an overview part. Articles I–III discuss WIMPs scattering off ^{83}Kr and ^{125}Te and articles IV and V discuss neutrino-nucleus scattering in context of Xe dark matter detectors. In the overview part the theoretical formalism and results of all five publications are drawn together in a coherent and concise manner.

Author Pekka Pirinen
Department of Physics
University of Jyväskylä
Finland

Supervisor Professor Jouni Suhonen
Department of Physics
University of Jyväskylä
Finland

Reviewers Professor Doron Gazit
Racah Institute of Physics
The Hebrew University of Jerusalem
Israel

Professor Theocharis Kosmas
Department of Physics
University of Ioannina
Greece

Opponent Professor Achim Schwenk
Institut für Kernphysik
Technische Universität Darmstadt
Germany

List of Publications

[I] J. D. Vergados, F. T. Avignone III, P. Pirinen, P. C. Srivastava, M. Kortelainen, and J. Suhonen, *Theoretical direct WIMP detection rates for transitions to the first excited state in* ^{83}Kr, *Phys. Rev. D* **92**, 015015 (2015).

[II] P. Pirinen, P. C. Srivastava, J. Suhonen, and M. Kortelainen, *Shell-model study on event rates of lightest supersymmetric particles scattering off* ^{83}Kr *and* ^{125}Te, *Phys. Rev. D* **93**, 095012 (2016).

[III] J. D. Vergados, F. T. Avignone III, M. Kortelainen, P. Pirinen, P. C. Srivastava, J. Suhonen, A. W. Thomas, *Inelastic WIMP-nucleus scattering to the first excited state in* ^{125}Te, *J. Phys. G: Nucl. Part. Phys.* **43**, 115002 (2016).

[IV] P. Pirinen, J. Suhonen, and E. Ydrefors, *Neutral-current neutrino-nucleus scattering off* Xe *isotopes*, *Adv. High Energy Phys.* **2018**, 9163586 (2018).

[V] P. Pirinen, J. Suhonen, and E. Ydrefors, *Charged-current neutrino-nucleus scattering off* Xe *isotopes*, submitted to Physical Review C (2018).

The author has performed part of the numerical calculations and participated in the writing of articles I and III. The author has carried out all the numerical calculations (except the shell-model calculations of article II) and written the first draft of articles II, IV, and V.

Contents

Chapter 1

Introduction

One of the most pressing current challenges in physics is to solve the problem of dark matter. From observation of galactic rotation curves [6–9], studies of structure formation [10, 11], and data from cosmic microwave background space missions [12, 13], it has become evident that the Universe is dominated by nonbaryonic cold dark matter (CDM) which outweighs the baryonic matter component at least fourfold. It is quite unacceptable to be in the dark about such a huge chunk of our Universe, and the dark matter hunt is running ever stronger in direct detection experiments.

The leading candidate for CDM is a relic of the big bang, very generally called the weakly interacting massive particle (WIMP). While acknowledging the multitude of possible WIMP scenarios [14–19], our analysis is motivated by the lightest supersymmetric particle (LSP) [20], which despite the null results of collider searches continues to be an appealing candidate to form the bulk of dark matter in the Universe. The LSP is thought to interact with normal atomic nuclei via spin-independent and spin-dependent interactions [21]. The spin-independent interaction should benefit of a coherent enhancement proportional to the square of the nuclear mass number. Being sensitive to spin-dependent interactions requires the nucleus to have a non-zero angular momentum, and for inelastic scattering to be possible, a low first excited state. As we do not know exactly how WIMPs and nuclei interact, it would be reasonable to have a target nucleus that is sensitive to both spin-independent and spin-dependent interactions in the elastic and inelastic channels.

Direct dark matter searches are founded on this idea of detecting the rare events of dark matter particles colliding with nuclei in the detector. As such, the experiments need to be run deep underground to minimize background radiation. The important role of nuclear structure in DM-nucleus scattering has been recognized for quite some time [21]. Popular target nuclei in current direct detection experiments include ^{19}F (PICO [22]), ^{23}Na (DAMA/LIBRA

[23], COSINE [24], KIMS [25]), ^{29}Si (SuperCDMS [26]) ^{73}Ge (SuperCDMS, EDELWEISS [27]) ^{127}I (DAMA/LIBRA, COSINE, KIMS), and ^{129,131}Xe (XENON [28], XMASS [29], LZ [30], PandaX [31]). Other proposed targets include ^{83}Kr and ^{125}Te, which are studied theoretically in this thesis. These nuclei are especially interesting due to their low first excited states, which could possibly be exploited via inelastic scattering of WIMPs.

In this thesis we present calculations of nuclear structure factors related to WIMP-nucleus scattering. The calculations were performed in the framework of the nuclear shell model. The early calculations of WIMP-nucleus scattering cross sections and event rates [32–34] handled the contribution of the nucleus within very simple models. In Ref. [35] the interacting boson-fermion model (IBFM) was used to examine spin-dependent WIMP-nucleus scattering. Various popular detector nuclei were analyzed in Ref. [36] in the MQPM (Microscopic Quasiparticle-Phonon Model) and in Refs. [37–44] in the nuclear shell-model. ^{125}Te was featured in an older shell-model study [45] but only in the context of spin-dependent elastic scattering. Progress has also been made in recent years in incorporating the effect of two-body currents of a chiral effective field theory approach into the nuclear spin structure functions in Refs. [41, 42, 44]. The nuclear responses in dark matter direct detection were formulated in a general non-relativistic effective theory in Refs. [46, 47]. In article [II] of the thesis we discuss the effects of nuclear structure of ^{83}Kr and ^{125}Te in elastic and inelastic scattering via spin-dependent and spin-independent interactions. In articles [I] and [III], we use the structure functions of article [II] to compute event rates for WIMP-nucleus scattering off ^{83}Kr and ^{125}Te focusing especially on inelastic scattering to the first excited state.

Direct dark matter detection experiments are expected to soon start seeing neutrinos as a background, which can in some cases very effectively mimic the recoil signal of WIMPs [48]. Solar neutrinos provide a constant source of such background neutrinos, and it is expected that neutrinos from the ^{8}B decay in the sun will be the first species of neutrinos detected in the next-generation dark matter detectors [49, 50]. In order to keep searching for weaker and weaker interacting WIMPs, a way to discriminate between dark matter and neutrino induced reactions in the detector must be found. The next-generation multi-ton liquid-xenon detectors (XENONnT, LZ, DARWIN) are expected to be among the first to hit the solar ^{8}B neutrino floor.

To that end, in the second part of this thesis we have examined neutrino-nucleus scattering off the most abundant xenon isotopes. In article [IV] we compute total cross sections for neutral-current scattering of solar ^{8}B neutrinos and supernova neutrinos off xenon isotopes of mass number $A = 128, 129, 130, 131, 132, 134, 136$. The computations were performed in the theoretical framework of the quasiparticle random-phase approximation (QRPA) for even-mass

nuclei, and in the microscopic quasiparticle-phonon model (MQPM) for odd-mass nuclei. The nuclear shell model was used for computation of the coherent elastic scattering cross sections for comparison with the QRPA results. In article [V] a similar analysis was performed for charged-current reactions involving the same xenon targets. The final states of the odd-odd nuclei were obtained within the proton-neutron QRPA (pnQRPA) formalism.

Similar calculations of neutrino-nucleus scattering cross sections in the QRPA and MQPM approach have been made for supernova neutrinos scattering off cadmium isotopes in Refs. [51, 52], molybdenum isotopes in Refs. [53–55], and lead isotopes in Ref. [56]. Recently a calculation of cross sections of charged-current scattering of supernova neutrinos and solar ^{8}B neutrinos off ^{40}Ar was performed in the nuclear shell model in Ref. [57]. Of the xenon isotopes, supernova neutrino scattering off ^{136}Xe has been examined earlier in Ref. [58], and charged-current reactions of ^{132}Xe in [59]. In addition, neutrino-nucleus scattering cross sections have been previously computed for various nuclei in the nuclear shell model [60–64], QRPA based on Skyrme forces [56, 61, 65, 66], QRPA with neutron-proton pairing [67–69], a consistent relativistic mean field approach [70, 71], and a hybrid model combining shell model for the allowed transitions and pnQRPA for forbidden transitions [72–74]. To our knowledge, this is the first calculation of neutrino-nucleus scattering cross sections for xenon isotopes other than ^{132}Xe and ^{136}Xe, and our results show some improvement even upon the previously computed cases.

The aim of this thesis is thus on one hand to investigate the potential of ^{83}Kr and ^{125}Te to be used to detect spin-dependent WIMP-nucleus interactions, and to provide predictions of neutrino-nucleus cross sections for xenon targets which can be useful in accounting for the neutrino floor. The results of this thesis may be of interest to the CUORE, DUNE, COHERENT, XENON, LZ, and DARWIN collaborations. The thesis is organized as follows. In Section 2 we introduce the nuclear models used in this work. In Section 3 we outline the formalism used for WIMP-nucleus scattering and present results for ^{83}Kr and ^{125}Te. In Section 4 we discuss neutrinos in the context of dark matter direct detection and present computed neutrino-nucleus scattering cross sections for the most abundant xenon isotopes. In Section 5 we summarize the main results of the thesis.

Chapter 2

Nuclear models

2.1 Nuclear mean field

Exactly solving the nuclear many-body problem is a formidable task even for very light nuclei. Tremendous progress is currently made in *ab initio* nuclear theories, which attempt to describe the nucleus from first principles. In the past such calculations were limited to light nuclei and some special cases. *Ab initio* calculations applying in-medium similarity renormalization group methods can at present be performed for open-shell nuclei even up to nuclei with $Z, N = 40$ [75]. However, for heavier complex nuclear systems some simplifying approximations on the nuclear interactions still have to be made. One such approximation is the nuclear mean field leading to the description of nuclear shell structure.

Instead of a system consisting of strongly interacting particles we can consider the nucleons to be mutually weakly interacting but moving in an external central mean field $v(\mathbf{r})$. The nuclear Hamiltonian of a nucleus of mass number A can then be written as [76]

$$H = T + V = \left[T + \sum_{i=1}^{A} v(\mathbf{r}_i) \right] + \left[V - \sum_{i=1}^{A} v(\mathbf{r}_i) \right] =: H_{\mathrm{MF}} + V_{\mathrm{RES}}, \quad (2.1)$$

where T is the kinetic energy, V is the potential energy, H_{MF} is the mean-field Hamiltonian and V_{RES} is a so-called residual two-body interaction. The handling of the mean-field Hamiltonian is straightforward, as its eigenvalue problem can be reduced to solving one-particle Schrödinger equations. Ideally the magnitude of the residual interaction should be reduced compared to the original potential V so that it can be handled as a small perturbation. Thus the optimal strategy is to choose a mean field that minimizes V_{RES}.

The mean-field hamiltonian can be obtained by a variational calculation through the iterative Hartree-Fock method. However, often a phenomenological potential is used instead. The most typical choice is probably the Woods-Saxon potential using the Bohr-Mottelson parameterization [77], which has been fitted to be quite accurate for nuclei close to the line of stability. A realistic mean field should also account for the Coulomb interaction between protons and the spin-orbit coupling. Along with the Pauli exclusion principle the mean-field potential gives rise to the nuclear shell structure with single-particle orbitals and energies correlating with experimentally observed magic numbers, i.e., closed shells of protons or neutrons.

Even with the mean-field approximation, the problem of diagonalizing the full Hamiltonian of Eq. (2.1) grows rapidly with increasing A. To this end, one must in most cases resort to the approximation of choosing a valence space of orbitals where nuclear excitations can take place. Outside of this valence space one has an inert core of filled orbitals of noninteracting nucleons and an external space of orbitals that are always empty. The approximation of an inert core is justified for describing the low-lying states of interest to the problem at hand. After choosing a valence space, one then needs to find an effective interaction to act as V_{RES} in that valence space. This valence-space interaction is often found by using a realistic two-body interaction potential and G-matrix methods [78] and/or by fitting two-body matrix elements to match experimental data regarding ground and excited-state properties of several nuclei in the valence space [79].

The nuclear shell model can be applied to nuclei quite close to having magic numbers of both protons and neutrons. Further away from closed shells, especially for heavier nuclei, other models must be relied on.

2.2 Quasiparticle random-phase approximation (QRPA)

Describing nuclei away from closed major shells can be a difficult task for models attempting to diagonalize the full nuclear Hamiltonian like the nuclear shell model. Therefore, some approximations need do be made in order to describe those nuclei reliably. One such approximation is the quasiparticle mean-field approach. A starting point for the quasiparticle framework is in the nuclear pairing phenomenon, where pairs of nucleons on a shell tend to couple to zero angular momentum.

Excited states of an even-even nucleus can be handled within the framework of the quasiparticle random phase approximation (QRPA). The starting point

of a QRPA calculation is in the BCS theory. The BCS theory was first built by Bardeen, Cooper, and Schrieffer [80] to describe the superconductivity in metals via the concept of Cooper pairs. An analogue in nuclear physics was soon found in the nuclear pairing interaction by Bohr, Mottelson, and Pines [81], and the BCS theory was considered suitable to be applied to nuclear structure physics. In the following we will present the essentials of the BCS and QRPA formalisms. We will use the Baranger notation, where $\alpha = (a, m_\alpha)$ and $a = (n_a, l_a, j_a)$.

The BCS vacuum is defined as [76]

$$|\mathrm{BCS}\rangle = \prod_{\alpha>0} (u_a - v_a A^\dagger_\alpha) \, |\mathrm{CORE}\rangle \,, \tag{2.2}$$

where u_a and v_a are variational parameters, $|\mathrm{CORE}\rangle$ is the inert core, i.e., the ground state of a doubly magic nucleus, and $A^\dagger_\alpha$ is the pair creation operator

$$A^\dagger_\alpha = c^\dagger_\alpha \tilde{c}^\dagger_\alpha, \tag{2.3}$$

where $c^\dagger_\alpha$ denotes the particle creation operator and $\tilde{c}^\dagger_\alpha = (-1)^{j_a+m_\alpha} c^\dagger_{-\alpha}$. The BCS vacuum of Eq. (2.2) is the vacuum for quasiparticles defined via the Bogoliubov-Valatin transformation

$$a^\dagger_\alpha = u_a c^\dagger_\alpha + v_a \tilde{c}_\alpha, \tag{2.4}$$

$$\tilde{a}_\alpha = u_a \tilde{c}_\alpha - v_a c^\dagger_\alpha, \tag{2.5}$$

where $a^\dagger_\alpha$ and $\tilde{a}_\alpha$ are the quasiparticle creation and annihilation operators, respectively.

The coefficients v_a and u_a obtain significance as the occupation and vacancy amplitudes of the orbital a. They are determined along with the single-quasiparticle energies from the BCS equations derived from a variational procedure through minimizing the energy of the BCS ground state $|\mathrm{BCS}\rangle$. The BCS state lacks good particle number, but the average particle number is used as a constraint in the variational procedure. The average particle number at the end of the iterative BCS calculation is required to be equal to the number of valence particles. This procedure is explained in detail in Ref. [76].

In the BCS calculation the lowest quasiparticle energy should be equal to the empirical pairing gap. This is achieved by scaling the interaction matrix elements by pairing strength parameters G^p_{pair} and G^n_{pair} for protons and neutrons separately. The empirical pairing gap can be computed by using

separation energies of the neighboring nuclei as [82]:

$$\Delta_{\rm p}(A,Z) = \frac{1}{4}(-1)^{Z+1}\big[S_{\rm p}(A+1,Z+1) - 2S_{\rm p}(A,Z) + S_{\rm p}(A-1,Z-1)\big], \tag{2.6}$$

$$\Delta_{\rm n}(A,Z) = \frac{1}{4}(-1)^{A-Z+1}\big[S_{\rm n}(A+1,Z) - 2S_{\rm n}(A,Z) + S_{\rm n}(A-1,Z)\big]. \tag{2.7}$$

This procedure cannot be followed for nuclei with magic numbers of protons or neutrons. For the magic species of nucleons the value of $G_{\rm pair} = 1.0$ is adopted and the sharp Fermi level of the particle-hole picture is recovered, i.e., $v_a = 1$ and $u_a = 0$ for orbitals below the Fermi level and $v_a = 0$ and $u_a = 1$ for levels above.

Taking the BCS state to be the ground state of an even-even nucleus, the wave functions of the excited states can be built by adding QRPA phonons. The basic QRPA excitation (phonon) to a state $\omega = (J_\omega, M_\omega, \pi_\omega, k_\omega)$ can then be written in terms of the BCS quasiparticles as

$$Q^\dagger_\omega = \sum_{a\le b} \mathcal{N}_{ab}(J_\omega)\left(X^\omega_{ab}[a^\dagger_a a^\dagger_b]_{J_\omega M_\omega} + Y^\omega_{ab}[\tilde{a}_a \tilde{a}_b]_{J_\omega M_\omega}\right), \tag{2.8}$$

where

$$\mathcal{N}_{ab}(J_\omega) = \frac{\sqrt{1+\delta_{ab}(-1)^{J_\omega}}}{1+\delta_{ab}} \tag{2.9}$$

is a normalization factor. It should be noted, that the BCS vacuum is not an exact vacuum for the QRPA phonons, but it can be used as a good approximation. The amplitudes X^ω_{ab} and Y^ω_{ab} describing the wave function of the excited state are solved from the QRPA equation

$$\begin{bmatrix} \mathrm{A} & \mathrm{B} \\ -\mathrm{B}^* & -\mathrm{A}^* \end{bmatrix} \begin{bmatrix} \mathrm{X}^\omega \\ \mathrm{Y}^\omega \end{bmatrix} = E_\omega \begin{bmatrix} \mathrm{X}^\omega \\ \mathrm{Y}^\omega \end{bmatrix}, \tag{2.10}$$

where the matrix A is a Tamm-Dankoff matrix and B is the so-called correlation matrix. The elements of the matrices can be written as

$$\begin{aligned} A_{ab,cd}(J) =& (E_a + E_b)\delta_{ac}\delta_{bd} + G_{\rm pp}(u_a u_b u_c u_d + v_a v_b v_c v_d)\langle ab; J|V|cd; J\rangle \\ &+ G_{\rm ph}\mathcal{N}_{ab}(J)\mathcal{N}_{cd}(J)\big[(u_a v_b u_c v_d + v_a u_b v_c u_d)\langle ab^{-1}; J|V_{\rm RES}|cd^{-1}; J\rangle \\ &- (-1)^{j_c+j_d+J}(u_a v_b v_c u_d + v_a u_b u_c v_d)\langle ab^{-1}; J|V_{\rm RES}|dc^{-1}; J\rangle\big], \end{aligned} \tag{2.11}$$

and

$$\begin{aligned} B_{ab,cd}(J) =& - G_{\rm pp}(u_a u_b v_c v_d + v_a v_b u_c u_d)\langle ab; J|V|cd; J\rangle \\ &+ G_{\rm ph}\mathcal{N}_{ab}(J)\mathcal{N}_{cd}(J)\big[(u_a v_b v_c u_d + v_a u_b u_c v_d)\langle ab^{-1}; J|V_{\rm RES}|cd^{-1}; J\rangle \\ &- (-1)^{j_c+j_d+J}(u_a v_b u_c v_d + v_a u_b v_c u_d)\langle ab^{-1}; J|V_{\rm RES}|dc^{-1}; J\rangle\big], \end{aligned} \tag{2.12}$$

where the coupled two-particle interaction matrix elements can be written as

$$\langle ab;J|V|cd;J\rangle = \mathcal{N}_{ab}(J)\mathcal{N}_{cd}(J)\sum_{\substack{m_\alpha m_\beta \\ m_\gamma m_\delta}}(j_a m_\alpha j_b m_\beta|JM)(j_c m_\alpha j_d m_\delta|JM)\bar{v}_{\alpha\beta\gamma\delta}. \tag{2.13}$$

In the above $\bar{v}_{\alpha\beta\gamma\delta}$ is the antisymmetrized and normalized two-nucleon interaction matrix element. The particle-hole matrix elements are obtained via the generalized Pandya transformation as

$$\langle ab^{-1};J|V_{\rm RES}|cd^{-1};J\rangle = \\ -\sum_{J'}\left[\mathcal{N}_{ad}(J')\mathcal{N}_{cb}(J')\right]^{-1}(2J'+1)\begin{Bmatrix} j_a & j_b & J \\ j_c & j_d & J' \end{Bmatrix}\langle ad;J'|V|cb;J'\rangle.$$

In Eqs. (2.11) and (2.12) the interaction matrix elements are scaled by the particle-particle and particle-hole strength parameters $G_{\rm pp}$ and $G_{\rm ph}$, respectively. The energies of especially the even-J positive-parity and odd-J negative-parity phonons are sensitive to the value of $G_{\rm ph}$. The energy of the first excited state of each J^π is fitted to an experimental value by altering the value of $G_{\rm ph}$, if such fit is possible. The energies of 0^+ states are also sensitive to the parameter $G_{\rm pp}$. As the first excited 0^+ state in the QRPA calculation is known to be spurious [51, 83], we use the parameters $G_{\rm ph}$ and $G_{\rm pp}$ to set the energy of the first excited 0^+ to zero and fitting the second 0^+ state to the experimental value of the first excited 0^+ state. The spurious first 0^+ state is then omitted from all subsequent calculations. The value of $G_{\rm pp} = 1$ was adopted for states of $J^\pi \neq 0^+$. The two-body interaction matrix elements of Eqs. (2.11) and (2.12) were derived from the Bonn A one-boson exchange potential.

We can similarly describe states in the odd-odd neighbors of the even-even reference nucleus in the proton-neutron QRPA (pnQRPA). The basic excitation (phonon) of the pnQRPA is similar to Eq. (2.8),

$$Q^\dagger_\omega = \sum_{pn}\left(X^\omega_{pn}[a^\dagger_p a^\dagger_n]_{J_\omega M_\omega} + Y^\omega_{pn}[\tilde{a}_p\tilde{a}_n]_{J_\omega M_\omega}\right), \tag{2.14}$$

and the X and Y amplitudes are solved from a matrix equation identical to Eq. (2.10) but the matrices A and B are adjusted to the proton-neutron picture. The (pn)QRPA formalism is derived in greater detail in Ref. [76].

It is also essential to renormalize the particle-particle and particle-hole interaction matrix elements in the pnQRPA with strength parameters $g_{\rm pp}$ and $g_{\rm ph}$ (lowercase to differentiate from the charge-conserving QRPA). The value of $g_{\rm ph}$ for the 1^+ multipole is chosen so that the energy of the Gamow-Teller

giant resonance (GTGR) approximately matches an empirical value given by a formula in Ref. [76]. An experimental value can also be used, but the energies of the GTGR are not known in many cases. The value of $g_{\rm pp}$ is important to the half-life of the beta decay of the first 1^+ state in odd-odd nuclei. In Ref. [84] a systematic study found the use of $g_{\rm pp} = 0.6 - 0.8$ justifiable for mass $A = 100 - 136$ nuclei and another analysis [85, 86] found $g_{\rm pp} = 0.63 \pm 0.17$ by studying some select medium-heavy nuclei. In this work we use $g_{\rm pp} = 0.60$ for the computation of 1^+ states in the pnQRPA, but the results of this thesis are not very sensitive to the value of this parameter.

2.3 Microscopic quasiparticle-phonon model (MQPM)

The microscopic quasiparticle-phonon model (MQPM) describes reliably the odd-mass nuclei based on a QRPA calculation for a neighbouring even-even reference nucleus. The states of the odd-mass nucleus can be described by one-quasiparticle excitations from the BCS vacuum, but in the MQPM, also three-quasiparticle configurations are accounted for. This is achieved by coupling a single quasiparticle with a QRPA phonon, and the MQPM excitation operator can be written as [87]

$$\Gamma_k^\dagger(jm) = \sum_n C_n^k a_{njm}^\dagger + \sum_{a,\omega} D_{a\omega}^k \left[a_a^\dagger Q_\omega^\dagger\right]_{jm}, \tag{2.15}$$

where $Q_\omega^\dagger$ is the QRPA excitation operator of Eq. (2.8). The MQPM relies on the same equations-of-motion method as the QRPA and this leads to the MQPM equations for the amplitudes C_n^k and $D_{a\omega}^k$ [87]:

$$\begin{bmatrix} \mathrm{A} & \mathrm{B} \\ \mathrm{B}^\intercal & -\mathrm{A}' \end{bmatrix} \begin{bmatrix} \mathrm{C}^k \\ \mathrm{D}^k \end{bmatrix} = E_k \begin{bmatrix} 1 & 0 \\ 0 & \mathrm{N} \end{bmatrix} \begin{bmatrix} \mathrm{C}^k \\ \mathrm{D}^k \end{bmatrix}, \tag{2.16}$$

where the matrices A, A′, and B contain information of the interaction between two one-quasiparticle states, two quasiparticle-phonon states, and one-quasiparticle and quasiparticle-phonon states, respectively. The matrix N is the overlap matrix between two three-quasiparticle states. The MQPM formalism is derived in detail in Ref. [87]. As mentioned earlier, the QRPA is known to produce some states that are spurious. In the MQPM calculations of this work the spurious first excited 0^+ state and the first 1^- state of the QRPA have been omitted in the calculations [51, 83, 88, 89].

Chapter 3

WIMP-nucleus scattering

Normal matter makes up only a rough fifth of all the matter in the Universe. In addition to normal matter, there exists a whole another dark world consisting of matter we know very little about. This dark matter has to be nonluminous, rather slow moving, and very weakly interacting with normal matter. While it is interesting to speculate on actual dark worlds like structures consisting for example of the hypothetical mirror matter [90], the current dark matter paradigm is new type of stable elementary particles which are gravitationally confined to the vicinity of galaxies. These new particles are generally referred to as weakly interacting massive particles (WIMPs). Another contender for dark matter are massive compact halo objects (MACHOs) such as brown dwarfs, black holes, and neutron stars. There has been a recent interest in primordial black holes making up the majority of dark matter [91]. In this work we focus on WIMPs and how they might be detected.

Extensions of the standard model of particle physics often naturally contain a WIMP that could be a candidate for dark matter. Perhaps the most popular such candidate is offered within the framework of supersymmetry (SUSY) [20]. SUSY relies on the existence of a new symmetry between bosonic and fermionic degrees of freedom. Provided that SUSY particles do not decay to standard-model particles, the lightest supersymmetric particle (LSP) should be stable. The LSP in many SUSY models is the lightest neutralino [20], which is a linear combination of the supersymmetric partners of the photon, Z boson, and the two neutral Higgs bosons. The neutralino as LSP would be weakly interacting and stable, and in many models the neutralino has a relic abundance suitable to be a good candidate for dark matter. This section is motivated by the idea of neutralino dark matter, but most of the discussion applies to general WIMPs as well.

How to detect a particle which clearly does not like to be seen? There are currently three strategies employed in the dark matter hunt. One is

searching for candidate particles in collider experiments [92]. That particle's existence within galaxies would then have to be proven by a different method. That method can be to look for indirect evidence of dark matter in areas of supposedly high dark-matter densities, e.g., the centers of galaxies (see Ref. [93] for a review of indirect dark matter searches). A surplus of gamma rays has been observed coming from the center of our galaxy [94] and this could be attributed to dark matter annihilating to known particles. These events typically happen very far away from Earth, and it is very difficult to say for certain that an indirect observation is in reality due to dark matter instead of a mimicing astrophysical source [93].

A real smoking-gun evidence of dark matter in our galaxy would be to detect a dark-matter particle bumping into an earthbound detector and producing an observable signal in a laboratory. After ruling out the possibility of the collisions being caused by a known species of particles, we are left with discovery of something new. This direct detection of dark matter is the current prevalent strategy for dark matter detection, supported by collider searches and indirect evidence.

Typically the direct detection experiments are based on the idea of WIMPs scattering coherently and elastically off a nucleus in the detector. If by some mechanism this elastic channel is forbidden, then new detection strategies need to be focused on. To this end, we examine two new candidates for target nuclei, ^{83}Kr and ^{125}Te, which have unusually low-lying excited states. We examine the potential of these excited states being used to detect inelastic scattering of WIMPs.

In this section we outline the theoretical formalism used to model WIMP-nucleus scattering and apply it to study elastic and inelastic scattering of WIMPs off ^{83}Kr and ^{125}Te. Underlying assumptions of the WIMP distribution in our local galactic neighborhood and the characteristic annual modulation signal in direct detection are also discussed.

3.1 WIMP distribution in our galaxy

Although the nature of dark matter is not known, we have some information on how it should be distributed within galaxies based on observations. There are two quantities that we are interested in. Firstly, the density of WIMPs in our neighborhood sets the scale for the number of possible scattering events taking place in a given time. Secondly, the velocity distribution of the WIMPs in part determines the shape of the recoil spectrum. The most commonly used model is the standard halo model (SHM), which assumes the dark matter to be distributed in an isothermal sphere, with a Maxwell-Boltzmann velocity

distribution

Many estimates of the dark matter density in the neighborhood of the Sun have been made, see Ref. [95] for a review. The values obtained over nearly a century of experiments range from $(0.0225 \pm 0.69)\ \mathrm{GeV/cm^3}$ to $(2.2 \pm 0.56)\ \mathrm{GeV/cm^3}$. More recently, the measurements have been converging towards a similar value near $0.3\ \mathrm{GeV/cm^3}$. In this work we adopt the benchmark value $\rho_0 = 0.3\,\mathrm{GeV/cm^3}$ for the local WIMP density. It should be noted that some uncertainty remains in the value of the dark matter density. However, as the value of $\rho_0 = 0.3\,\mathrm{GeV/cm^3}$ has been adopted quite universally across the field, the results presented in this thesis will be widely comparable to other works.

Adopting the standard halo model, we use a Maxwell-Boltzmann distribution to model the velocity distribution of WIMPs in our galaxy. The velocity distribution is expressed as

$$f\left(\mathbf{v}, \mathbf{v}_{\mathrm{E}}\right) = \left(\sqrt{\pi} v_0\right)^{-3} e^{-(\mathbf{v}+\mathbf{v}_{\mathrm{E}})^2/v_0^2}, \tag{3.1}$$

where $\mathbf{v}$ is the WIMP velocity relative to the Earth, $\mathbf{v}_{\mathrm{E}}$ is the velocity of the earth relative to the galactic center, and v_0 is the speed of the sun with respect to the galactic center. A sharp cutoff to the distribution is imposed by the local galactic escape speed v_{esc}. We connect the velocity of the Earth to the velocity of the Sun by writing

$$\mathbf{v}_{\mathrm{E}} = \mathbf{v_0} + \mathbf{v_1}, \tag{3.2}$$

where $\mathbf{v_1}$ is the velocity of the Earth with respect to the Sun. By writing the velocity distribution in this form we can analyze the effects of the seasonal differences in the Earth's velocity, i.e., annual modulation in dark matter direct detection (see section 3.2). By aligning our coordinate system so that $\widehat{\mathbf{x}}_2$ points to the galactic north, $\widehat{\mathbf{x}}_3$ in the direction of the Sun's velocity, and $\widehat{\mathbf{x}}_1 = \widehat{\mathbf{x}}_2 \times \widehat{\mathbf{x}}_3$, we can write

$$\mathbf{v_1} = v_1 \left[\sin(\alpha)\widehat{\mathbf{x}}_1 - \cos(\alpha)\cos(\gamma)\widehat{\mathbf{x}}_2 + \cos(\alpha)\sin(\gamma)\widehat{\mathbf{x}}_3\right], \tag{3.3}$$

where $v_1 = 30\,\mathrm{km/s}$ and γ is the angle between the normal of the ecliptic and the galactic plane ($\gamma \approx 29.8°$). α is the phase of the Earth's orbit, i.e., $\alpha = 0°$ on June 2 and $\alpha = 180°$ on December 2.

In this work we use the standard value of $v_0 = 220\,\mathrm{km/s}$ [96] and a conservative upper limit of $v_{\mathrm{esc}} = 625\mathrm{km/s}$ [97]. There remain sizable uncertainties in these parameters, however. The escape speed v_{esc} practically only affects the tail of the Maxwell-Boltzmann distribution, and even quite large changes in v_{esc} do not bring about significant changes in our results. However, the

calculations are somewhat more sensitive to the value of v_0. The value of v_0 has been estimated to lie between (200 ± 20) and (279 ± 33) km/s [98]. Another estimate gives (254 ± 16) km/s [99]. For the local escape velocity, the RAVE survey gives the estimate $v_{\text{esc}} = 537^{+59}_{-43}$ km/s [100].

3.2 Annual modulation

As our solar system moves in the galactic dark matter halo, there is an effective WIMP "wind" flowing through the solar system. Adding to this the movement of the Earth around the Sun in accordance to Eq. (3.3), it appears that the WIMP wind should be strongest when the velocities v_0 and v_1 are the most parallel ($\alpha = 0°$, in June) and weakest when they are the most antiparallel ($\alpha = 180°$, December). This is illustrated in Fig. 3.1. We would thus expect to encounter WIMPs at a higher rate around June than in December. This effect is known as annual modulation in direct dark matter detection.

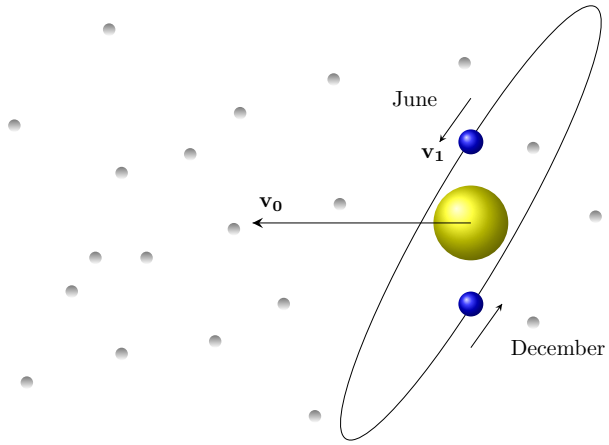

Figure 3.1. Schematic figure of the relative motion of the Sun and Earth giving rise to the annual modulation in the dark matter direct detection event rate. In June the relative motion of the Earth with respect to the Sun is the most aligned with the velocity of the Sun, while in December the direction of the Earth with respect to the Sun is the opposite.

Annual modulation can be used as an efficient detection strategy. The DAMA collaboration has observed an annual modulation in their detector signal over two decades [23]. At present date the statistical significance of the DAMA modulation signal is 9.5σ in the energy region of (1–6) keV [23]. However, the modulation has not been unambiguously proven to be due to

dark matter. The DAMA results appear to be in strong tension with other experiments that have ruled out the cross section range the DAMA result would indicate [101, 102]. There is a massive ongoing experimental effort to verify or nullify the DAMA result in the SABRE collaboration [103]. They plan to operate two DAMA-like detectors, one on the northern hemisphere and one on the southern hemisphere. If both detectors were to show similar annual modulation, then there is little room for the signal to be anything else but dark matter.

Annual modulation is thus an important characteristic to consider in WIMP-nucleus scattering. In the following section we will outline the formalism for the WIMP-nucleus scattering event rate, where we have also included the effects of annual modulation.

3.3 LSP-nucleus scattering

For a detector containing a mass of m_{det} of the target material, the LSP-nucleus total event rate can be expressed as [39]

$$\langle R\rangle = \left[\left(f_{\text{A}}^0\right)^2 D_1 + 2 f_{\text{A}}^0 f_{\text{A}}^1 D_2 + \left(f_{\text{A}}^1\right)^2 D_3 + A^2 \left(f_{\text{S}}^0 - f_{\text{S}}^1 \frac{A-2Z}{A} \right)^2 D_4 \right] m_{\text{det}}[\text{kg}]. \tag{3.4}$$

Here the nuclear structure and seasonal modulation effects are contained in the integrated nuclear structure factors D_n, while particle-physics effects from supersymmetry reside in the scalar and axial-vector form factors f_{S}^ρ and f_{A}^ρ. Furthermore, the interaction between the LSP and the nucleus is considered either spin-dependent or spin-independent, depending on whether the spin operator is present. The expression of Eq. (3.4) can thus also be divided into a spin-dependent part containing the axial-vector terms, and a spin-independent part containing the scalar terms.

It should be noted that the expression of Eq. (3.4) is an approximation neglecting the contributions from vector, pseudoscalar, and tensor currents [38]. The effects of two-body currents predicted in chiral effective field theory have been studied in detail in Refs. [41, 42, 44]. It appears that the two-body currents, when accounted for, have a tendency to decrease the axial part of the current [44]. In this thesis we have only included the effects of one-body currents, but the inclusion of two-body currents should not affect the main qualitative conclusions drawn in this work.

Let us look into the integrated nuclear structure factors D_n of Eq. (3.4). We define what we call a modulation function G as a function of $\psi = v/v_0$

and $\xi = \cos\theta$, the cosine of the angle between $\mathbf{v}$ and $\mathbf{v}_{\rm E}$, as

$$G(\psi,\xi) = \frac{\rho_0}{m_\chi}\frac{\sigma_0}{A m_{\rm p}}\left(\frac{1}{m_{\rm p} b}\right)^2 \frac{e^{-\lambda^2}}{\sqrt{\pi}}\frac{c^2}{v_0}\psi e^{-\psi^2} e^{-2\lambda\psi\xi}\,, \tag{3.5}$$

where $\rho_0 = 0.3\,\mathrm{GeV/cm^3}$ is the local WIMP density, $\sigma_0 = \frac{1}{2\pi}(G_{\rm F} m_{\rm p})^2 \approx 0.77\times 10^{-38}\,\mathrm{cm}^2$, $m_{\rm p}$ the mass of a proton, $G_{\rm F}$ the Fermi coupling constant, m_χ the LSP mass, b the harmonic oscillator length of the target nucleus, and $\lambda = v_{\rm E}/v_0$. The modulation function by definition contains all the information of the WIMP velocity distribution, and thus the effects of annual modulation.

Another ingredient entering the D_n factors is a spin structure function

$$F_{\rho\rho'}(u) = \sum_{\lambda,\kappa}\frac{\Omega_\rho^{(\lambda,\kappa)}(u)\Omega_{\rho'}^{(\lambda,\kappa)}(u)}{\Omega_\rho\Omega_{\rho'}}\,, \tag{3.6}$$

where

$$\Omega_\rho = \Omega_\rho^{(0,1)}(0) \tag{3.7}$$

are called the static spin matrix elements (SSMEs), and

$$\Omega_\rho^{(\lambda,\kappa)}(u) = \sqrt{\frac{4\pi}{2J_i+1}}\left\langle J_f\left|\left|\sum_{j=1}^{A}\left[\mathbf{Y}_\lambda(\Omega_j)\otimes\sigma\right]_\kappa j_\lambda(\sqrt{u}r_j)\omega_\rho(j)\right|\right|J_i\right\rangle. \tag{3.8}$$

Here the index j runs over all nucleons in the target nucleus, $\mathbf{Y}_\lambda$ is a vector spherical harmonic, Ω_j is a solid angle related to the position of the nucleon, σ is the spin operator, j_λ is a spherical Bessel function, $\omega_0(j) = 1$, and $\omega_1(j) = \tau_3(j)$ is the third component of isospin. u is the momentum transfer q expressed in dimensionless units $u = q^2b^2/2$ and it can thus also be written in terms of the nuclear recoil energy $E_{\rm R}$ as $u = A m_{\rm p} b^2 E_{\rm R}$. Note that the above definition (3.6) of the SSFs is normalized to unity at zero momentum transfer. We would like to note that many authors use spin structure functions which are not normalized in this manner. Our structure functions $F_{\rho\rho'}$ relate to the commonly used $S_{\rho\rho'}$ functions [21] simply as

$$S_{00}(u) = \frac{2J_i+1}{16\pi}\Omega_0^2 F_{00}(u)\,, \tag{3.9}$$

$$S_{01}(u) = \frac{2J_i+1}{8\pi}\Omega_0\Omega_1 F_{01}(u)\,, \tag{3.10}$$

$$S_{11}(u) = \frac{2J_i+1}{16\pi}\Omega_1^2 F_{11}(u)\,. \tag{3.11}$$

The integrated nuclear-structure factors of Eq. (3.4) can then be expressed in terms of Eqs. (3.5), (3.6), and (3.7) as

$$D_1 = \int_{-1}^{1} \int_{\psi_{\min}}^{\psi_{\max}} \int_{u_{\min}}^{u_{\max}} G(\psi,\xi) F_{00}(u) \Omega_0^2 d\xi d\psi du \,, \tag{3.12}$$

$$D_2 = \int_{-1}^{1} \int_{\psi_{\min}}^{\psi_{\max}} \int_{u_{\min}}^{u_{\max}} G(\psi,\xi) F_{01}(u) \Omega_0 \Omega_1 d\xi d\psi du \,, \tag{3.13}$$

$$D_3 = \int_{-1}^{1} \int_{\psi_{\min}}^{\psi_{\max}} \int_{u_{\min}}^{u_{\max}} G(\psi,\xi) F_{11}(u) \Omega_1^2 d\xi d\psi du \,, \tag{3.14}$$

$$D_4 = \int_{-1}^{1} \int_{\psi_{\min}}^{\psi_{\max}} \int_{u_{\min}}^{u_{\max}} G(\psi,\xi) \left|F(u)\right|^2 d\xi d\psi du \,. \tag{3.15}$$

In the nuclear structure factor of the coherent channel, Eq. (3.15), $F(u)$ is the nuclear form factor. The limits of integration are set on one hand by demanding that the speed of the WIMP must be enough to give a recoil greater than the detector threshold energy $Q_{\rm thr}$ in an elastic collision with a nucleus in the detector, and on the other hand by demanding that the WIMPs are gravitationally confined into our galaxy, i.e., their velocity cannot exceed the local galactic escape velocity $v_{\rm esc}$. Therefore the limits are

$$\psi_{\min} = \frac{c}{v_0} \left(\frac{A m_{\rm p} Q_{\rm thr}}{2\mu_r^2} \right)^{1/2} \,, \tag{3.16}$$

$$\psi_{\max} = -\lambda\xi + \sqrt{\lambda^2\xi^2 + \frac{v_{\rm esc}^2}{v_0^2} - 1 - \frac{v_1^2}{v_0^2} - \frac{2 v_0 v_1}{v_0^2} \sin\gamma \cos\alpha} \,, \tag{3.17}$$

$$u_{\min} = A m_{\rm p} Q_{\rm thr} b^2 \,, \tag{3.18}$$

$$u_{\max} = 2 \left(\psi \mu_r b v_0 / c\right)^2 \,, \tag{3.19}$$

where μ_r is the reduced mass of the WIMP-nucleus system.

The event rate of inelastic scattering looks very similar to the elastic case and it can be written as

$$\langle R \rangle_{\rm inel} = \left[\left(f_{\rm A}^0\right)^2 E_1 + 2 f_{\rm A}^0 f_{\rm A}^1 E_2 + \left(f_{\rm A}^1\right)^2 E_3 \right] m_{\rm det}[\rm kg] \,, \tag{3.20}$$

where we now label the integrated nuclear structure factors E_n to distinguish them from the D_n coefficients of elastic scattering although their definition

looks exactly the same, i.e., the definition of Eqs. (3.12)-(3.14) hold for the corresponding E_n coefficients. However, SSMEs and SSFs corresponding to the transition to the excited state must be used and the kinematics are modified so that the integration limits are different. For a final excited state of energy E^* the limits become

$$u_{\rm min} = \frac{1}{2} b^2 \mu_r^2 \frac{v_0^2}{c^2} \psi^2 \left[1 - \sqrt{1 - \Gamma/\psi^2}\right]^2 , \tag{3.21}$$

$$u_{\rm max} = \frac{1}{2} b^2 \mu_r^2 \frac{v_0^2}{c^2} \psi^2 \left[1 + \sqrt{1 - \Gamma/\psi^2}\right]^2 , \tag{3.22}$$

$$\psi_{\rm min} = \sqrt{\Gamma} , \tag{3.23}$$

$$\psi_{\rm max} = -\lambda\xi + \sqrt{\lambda^2\xi^2 + \frac{v_{\rm esc}^2}{v_0^2} - 1 - \frac{v_1^2}{v_0^2} - \frac{2 v_0 v_1}{v_0^2} \sin\gamma \cos\alpha} , \tag{3.24}$$

$$\tag{3.25}$$

where

$$\Gamma = \frac{2E^*}{\mu_r c^2} \frac{c^2}{v_0^2} . \tag{3.26}$$

Another way to approach the WIMP-nucleus scattering problem is to write the spin-dependent elastic scattering differential event rate for a target of mass $m_{\rm t}$ as [104]

$$\left.\frac{dR_0}{dE_{\rm R}}\right|_A = \frac{\rho_0}{m_\chi} \frac{m_{\rm t}}{A m_{\rm p}} \left(\frac{\mu_{\rm r}}{\mu_{\rm p}}\right)^2 \sqrt{\langle v^2 \rangle} m_p A b^2 \sigma_A^{\rm spin} \left.\left(\frac{dt}{du}\right)\right|_{\rm spin} , \tag{3.27}$$

where

$$\left.\left(\frac{dt}{du}\right)\right|_{\rm spin} = \frac{\sqrt{2}}{3} a^2 F_{11}(u) \Psi_0(a\sqrt{u}) \tag{3.28}$$

contains information of the nuclear structure in $F_{11}(u)$ and Ψ_0 is a function dependent on the velocity distribution. Here $a = (\sqrt{2}\mu_r v_0 b)^{-1}$ and $a\sqrt{u}$ corresponds to the minimum velocity for a given energy transfer divided by v_0. The function Ψ_0 is defined as $\Psi_0(v_{\rm min}/v_0) = g(v_{\rm min}, v_{\rm E})/v_0$, where for the Maxwell-Boltzmann distribution

$$g(v_{\rm min}, v_{\rm E}) = \frac{1}{(\sqrt{\pi} v_0)^3} \int_{v_{\rm min}}^{v_{\rm max}} e^{-(v^2 + 2\mathbf{v}\cdot\mathbf{v}_{\rm E} + v_{\rm E}^2)/v_0} v dv d\Omega. \tag{3.29}$$

It should be noted that Eq. (3.27) gives the time-averaged event rate where the effect of annual modulation is not included. The nuclear static spin

cross section appearing in Eq. (3.27) can be written as

$$\sigma_A^{\rm spin} = \left(1 + 2{\rm sign}(a_1 a_0)\frac{F_{01}(u)}{F_{11}(u)}\sqrt{\frac{\sigma_0(N)}{\sigma_1(N)}} + \frac{F_{00}(u)}{F_{11}(u)}\frac{\Omega_0^2\sigma_0(N)}{\Omega_1^2\sigma_1(N)}\right)\frac{\Omega_1^2\sigma_1(N)}{3}. \tag{3.30}$$

where the amplitudes a_0 and a_1 depend on the WIMP model and the quark model for the nucleons [104]. We assume ${\rm sign}(a_1 a_0) = +1$ in this work. $\sigma_0(N)$ and $\sigma_1(N)$ are the isoscalar and isovector elementary nucleon cross sections, respectively. If the isoscalar nucleon cross section is suppressed, as it is expected to be in many models [104], equation (3.30) simplifies to

$$\sigma_A^{\rm spin} \approx \frac{\Omega_1^2\sigma_1(N)}{3}. \tag{3.31}$$

This way one can factor out the unknown particle physics into the isovector nucleon cross section, and for non-zero $\sigma_0(N)$ also into the ratio $\sigma_0(N)/\sigma_1(N)$, which can then be used as model parameters to estimate event rates for WIMP-nucleus scattering. This procedure is followed in articles [I] and [III] of this thesis. The differential event rate for inelastic scattering to an excited state of energy $E_{\rm ex}$ is of the same form as Eq. (3.27), but with kinematics modified similarly as before. One should also use SSMEs and SSFs corresponding to the transition to the excited state in Eq. (3.30) and substitute $\psi_0(a\sqrt{u}) \to \psi_0(a(u + \mu_r E_{\rm ex} b^2)/\sqrt{u})$ in Eq. (3.28).

3.4 Results

In article [II] we performed nuclear-structure calculations in the nuclear shell model to investigate WIMP-nucleus scattering off ^{83}Kr and ^{125}Te. All shell-model calculations were made by using the shell-model code NuShellX@MSU [105]. The calculation for ^{83}Kr was made using the jj44b effective interaction [106] in the 28–50 valence space. For ^{125}Te we used the SN100PN interaction [78] in the 50–82 valence shell. For ^{83}Kr we were able to perform the calculation in the full valence space, but for ^{125}Te we had to truncate the model space to keep the matrix dimension in the calculation manageable. Therefore, for ^{125}Te, we allowed valence protons to only occupy the $\pi 0g_{9/2}$ and $\pi 1d_5/2$ orbitals. For neutrons we demanded that the $\nu 0g_{9/2}$ and $\nu 1d_{5/2}$ orbitals are completely filled, and in addition we set a minimum of six neutrons on the $\nu 0h_{11/2}$ orbital.

In Fig. 3.2 we present the computed and experimental energy spectra for ^{83}Ke and ^{125}Te. It appears that a problem with negative-parity states exists in both effective interactions, and negative-parity states are predicted much lower in energy than in the experimental spectrum. However, the order of the

positive-parity states of interest is correct in the calculations for both ^{83}Kr and ^{125}Te.

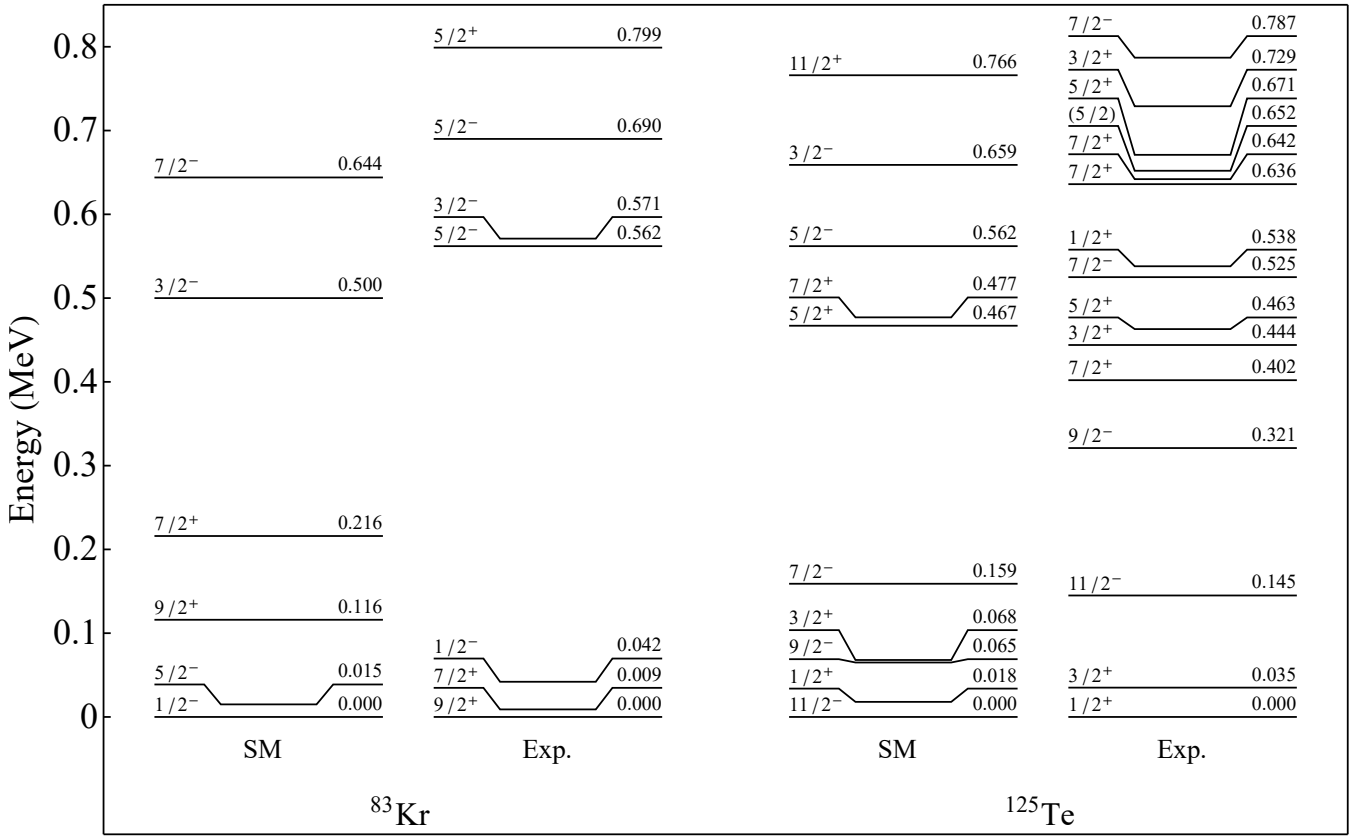

Figure 3.2. Experimental (Exp.) and shell-model computed (SM) energy levels of ^{83}Kr and ^{125}Te.

We also performed a set of calculations with different model space truncations, in which we noticed that small changes in the truncation do not have a massive effect on the final LSP-nucleus scattering results. For ^{83}Kr we also performed a calculation with a different effective interaction, JUN45 [79]. The JUN45 interaction reproduced the experimental energy spectrum quite well, but predicted a vanishingly small M1 transition strength compared to the experimental value for the transition from the first excited state to the ground state. In table 3.1 we show the computed and experimental ground-state and first-excited-state magnetic moments and B(M1) transition strengths from the first excited state to the ground state for ^{83}Kr and ^{125}Te. The results for ^{83}Kr using the jj44b interaction are in reasonable agreement with experiment,

as are those for ^{125}Te. However, the magnetic moments are in general overestimated in magnitude, and the M1 transition strengths underestimated. Similar accuracy can be expected of our results for WIMP-nucleus scattering. As the operators involved in inelastic WIMP-nucleus scattering and M1 gamma transitions, are similar, results obtained for ^{83}Kr using the JUN45 interaction could not be trusted and we used the jj44b interaction instead, despite the poorer energy spectrum reproduction.

Table 3.1. Ground-state and first-excited-state magnetic moments μ (in μ_N) and B(M1) transition strengths (in W.u.) from the first excited state to the ground state of ^{83}Kr and ^{125}Te compared between the shell-model calculations and experiment. For ^{83}Kr, results for the two interactions jj44b and JUN45 are listed.

Nucleus	Setup	μ(gs)	μ(1st exc)	B(M1)
^{83}Kr	Experimental	-0.970669(3)	-0.943(2)	0.00933(4)
	jj44b	-1.412	-1.099	0.0028
	JUN45	-1.457	-1.185	0.0000
^{125}Te	Experimental	-0.8885051(4)	0.605(4)	0.0226(4)
	SN100PN	-1.598	0.950	0.00564

The static spin matrix elements (SSMEs) for elastic and inelastic scattering of WIMPs off ^{83}Kr and ^{125}Te are given in Table 3.2. We can see that the values for ^{125}Te are larger and judging purely by the SSMEs it would already appear that ^{125}Te is a more suitable WIMP detector. Moreover, in the coherent channel ^{125}Te also benefits of the A^2 enhancement due to its larger mass. Even though ^{83}Kr has a kinematic advantage of the lower first excited state in inelastic scattering, this cannot overcome the hindrance provided by the small SSME.

Table 3.2. Static spin matrix elements for elastic and inelastic LSP-nucleus scattering off ^{83}Kr and ^{125}Te.

Nucleus	$\Omega_0^{\rm el}$	$\Omega_1^{\rm el}$	$\Omega_0^{\rm inel}$	$\Omega_1^{\rm inel}$
^{83}Kr	1.037	-1.018	-0.048	0.044
^{125}Te	1.456	-1.502	-0.157	0.196

In Fig. 3.3 we present the spin structure functions for ^{83}Kr and ^{125}Te for elastic scattering, and Fig. 3.4 shows the same for inelastic scattering. For elastic scattering the SSFs initially fall fast with increasing momentum

transfer and they follow quite closely the square of the nuclear form factor at $0 \leq u \leq 1$. A noteworthy feature is that the SSFs F_{00}, F_{01}, and F_{11} are nearly equal for elastic scattering. For inelastic scattering the situation is different, and the different SSFs for both ^{83}Kr and ^{125}Te differ somewhat around $u \approx 1$. The SSFs for ^{125}Te start with an upward slope, which reflects better sensitivity to the spin-dependent interaction.

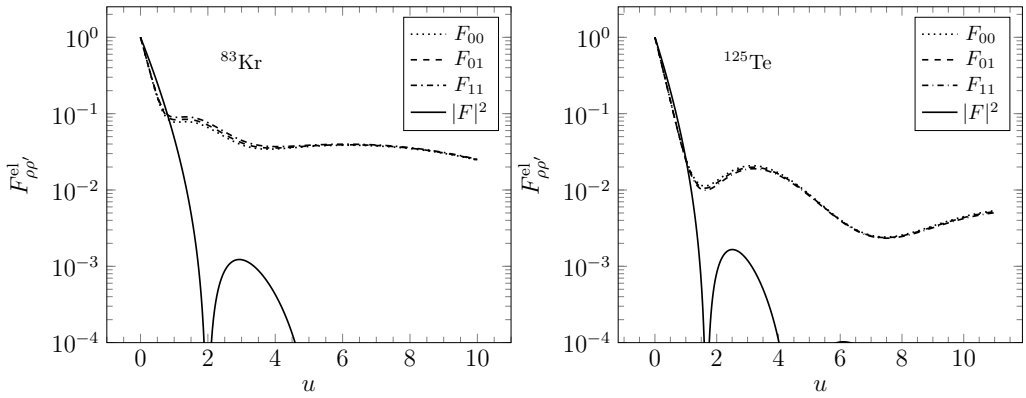

Figure 3.3. Spin structure functions and square of the nuclear form factor for elastic scattering of WIMPs off ^{83}Kr (left panel) and ^{125}Te (right panel).

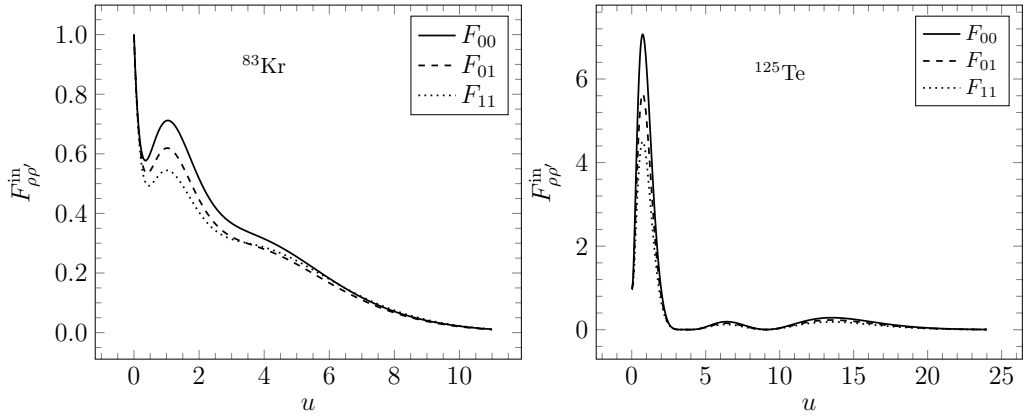

Figure 3.4. Spin structure functions for inelastic scattering of WIMPs off ^{83}Kr (left panel) and ^{125}Te (right panel).

We present the D_n coefficients of elastic scattering for ^{83}Kr and ^{125}Te in Figs. 3.5 and 3.6, respectively. The effect of the detector threshold energy has a large influence on the D_n coefficients, and thus the total event rate of elastic scattering, as seen in these figures. For ^{125}Te the coefficients of the spin-dependent channel are larger than for ^{83}Kr, but the spin-independent D_4

is larger for ^{83}Kr than for ^{125}Te. This is not enough, however, to overcome the A^2 enhancement in the event rate which benefits the heavier ^{125}Te. Looking at the D_n coefficients, the largest event rates would be expected for WIMPs of mass $m_\chi \approx 30 - 60\,\mathrm{GeV}$, depending on the detector threshold. Annual modulation is represented by the thickness of the curves, and its amplitude seems to be of the order of a few percent of the total value of the D_n coefficients, which should reflect similarly to the total event rate.

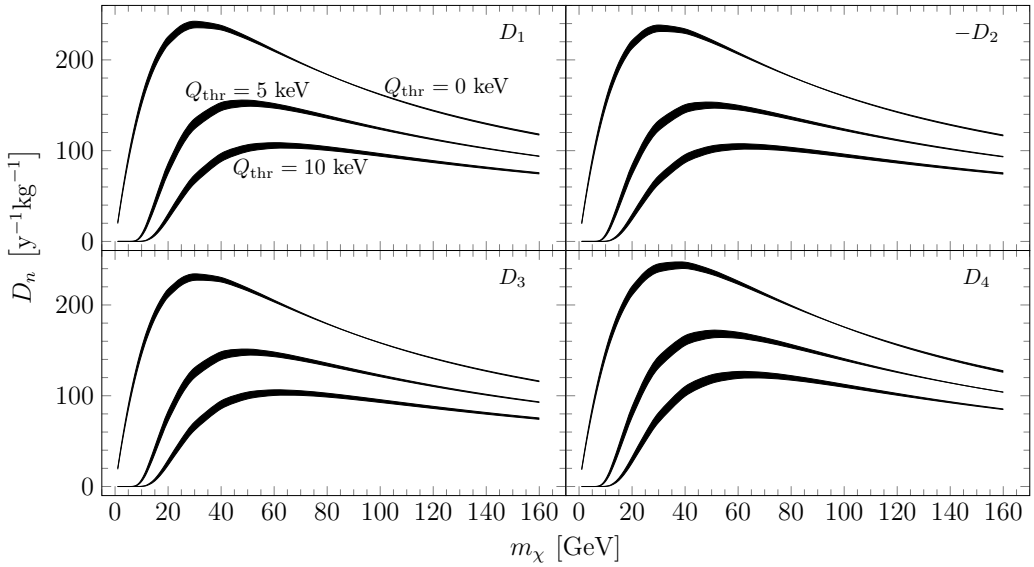

Figure 3.5. Nuclear-structure coefficients D_n of Eqs. (3.12)–(3.15) for elastic scattering of WIMPs off ^{83}Kr. The top, middle, and bottom curves were calculated with threshold energies $Q_{\mathrm{thr}} = 0, 5, 10\,\mathrm{keV}$, respectively. The thickness of the curves represents the effect of annual modulation. Note that the absolute value of the coefficient D_2 is shown.

The E_n coefficients of inelastic scattering as a function of the LSP mass are shown in Figs. 3.7 and 3.8 for ^{83}Kr and ^{125}Te, respectively. As can be seen, the coefficients of ^{125}Te are almost two orders of magnitude larger than those of ^{83}Kr. Also the peak of the graphs is at a higher WIMP mass than for elastic scattering, roughly 100 GeV for ^{83}Kr and 150 GeV for ^{125}Te. Another important observation is that the amplitude of the annual modulation is more visible in the inelastic channel. The E_n coefficients drop rapidly at smaller LSP masses, but given a sufficiently heavy LSP the nuclear response of ^{125}Te could provide new opportunities for WIMP searches.

It should be noted that the above examination only relies on nuclear physics and assumptions of the dark matter distribution. No assumptions are made about the WIMP-nucleus couplings, other than that the interaction

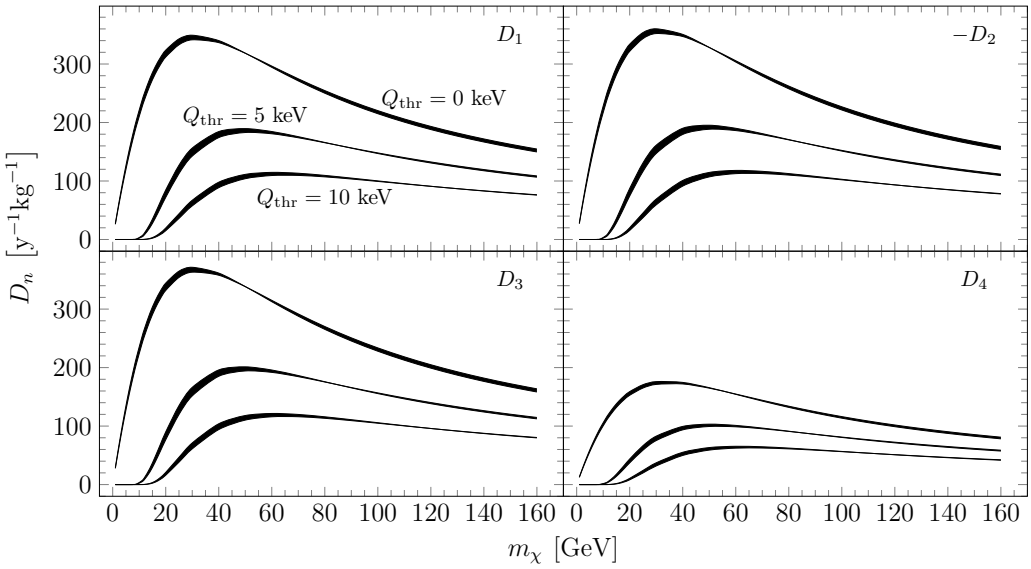

Figure 3.6. The same as Fig. 3.5 for elastic scattering of WIMPs off ^{125}Te.

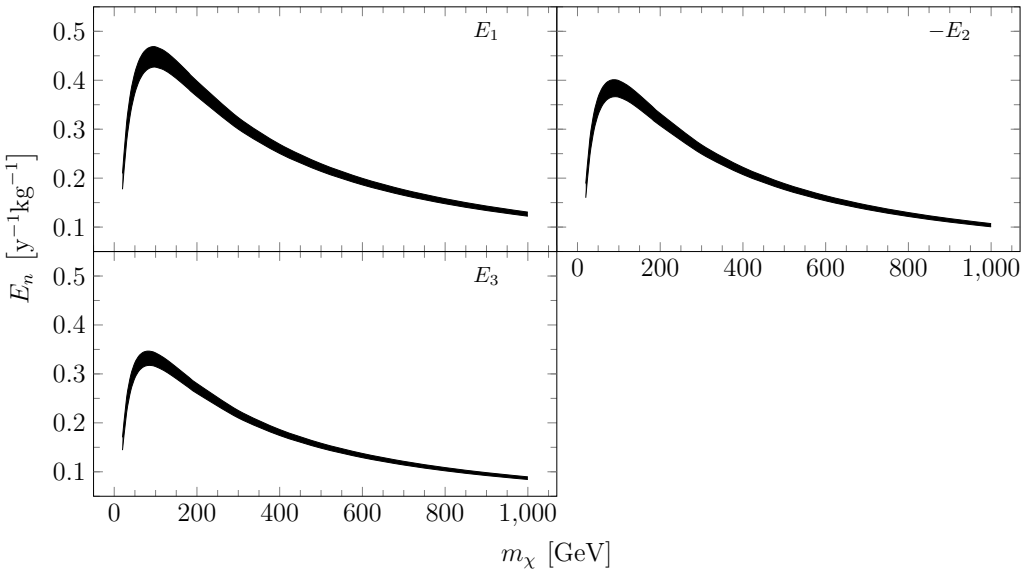

Figure 3.7. Nuclear-structure coefficients E_n for inelastic scattering of WIMPs off ^{83}Kr. The thickness of the curves represents the effect of annual modulation. Note that the absolute value of the coefficient E_2 is shown.

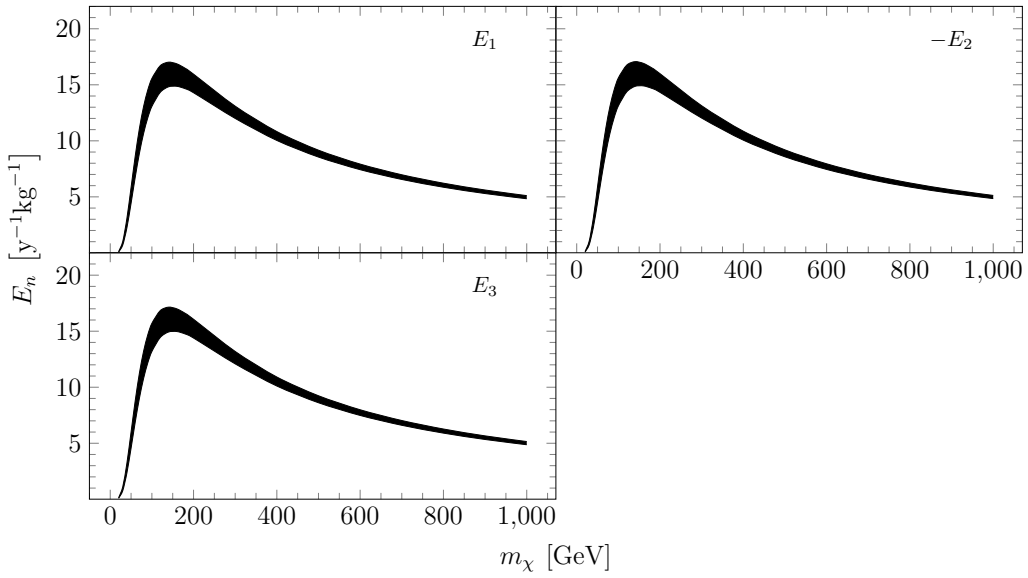

Figure 3.8. The same as Fig. 3.7 for inelastic scattering of WIMPs off ^{125}Te.

can be divided into the conventional spin-dependent and spin-independent parts. The results are thus valid for the LSP, but also essentially for any WIMP that interacts with matter dominantly through the spin-dependent and spin-independent channel. To compute the total event rates one also needs the particle-physics input, which in the case of the LSP means the $f_{\rm A}^{\rho}$ and $f_{\rm S}^{\rho}$ coefficients of Eq. (3.4). Some evaluations of these parameters have been made for several sets of supersymmetric parametrizations in Ref. [108, 109]. However, most if not all of those SUSY solutions have been made obsolete by collider searches and direct detection limits.

In article [I] we performed an analysis of spin-dependent WIMP-nucleus scattering event rates for a ^{83}Kr target based on the shell-model calculation described above. Instead of choosing a particle-physics model for WIMP-nucleus interactions, the elementary WIMP-nucleon isovector cross section was taken as an input parameter. The value of $\sigma_1(N) = 17$ fb [110] was adopted for the spin-dependent WIMP-nucleon isovector cross section. Although the value of the WIMP-nucleon cross section was inspired by a spin-3/2 Majorana dark matter candidate, no other commitment to a specific model was made. In article [I] we assumed the isovector cross section to be dominant, and set the value of the elementary isoscalar WIMP-nucleon cross section to zero.

We were then able to estimate the spin-dependent differential event rate with respect to the recoil energy $E_{\rm R}$ for WIMP-nucleus scattering off ^{83}Kr. The results are shown in Fig. 3.9 for elastic scattering in panel (a) and inelastic scattering in panel (b). Note that the spin-independent coherent

channel has been omitted from this examination. It is quite evident from Fig. 3.9 that the inelastic channel is heavily suppressed compared to the elastic channel. However, the spectral shape is somewhat different as the inelastic event rate vanishes at zero recoil energy. The shape of the spectrum could in principle be used to differentiate between the elastic and inelastic channel.

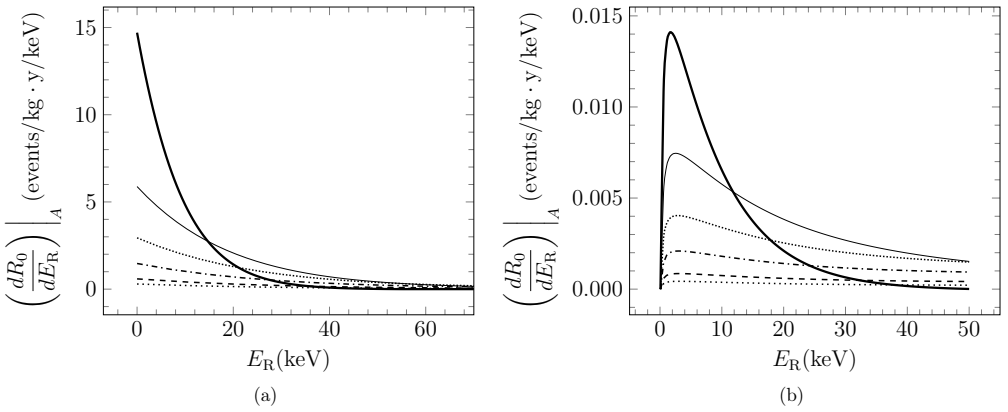

Figure 3.9. Differential event rate with respect to the recoil energy E_{R} for WIMPs of select masses scattering off a ^{83}Kr target (a) elastically and (b) inelastically. Only spin-dependent scattering is included. The thick solid, solid, dotted, dashed-dotted, dashed, and loosely dotted lines correspond to WIMP masses of 20, 50, 100, 200, 500, and 1000 GeV, respectively.

The time-averaged total event rate, i.e., the event rate averaged over the annual modulation for elastic and inelastic scattering of WIMPs off a ^{83}Kr target are given in Fig. 3.10 as a function of the WIMP mass. The event rates for inelastic scattering are much smaller than for elastic scattering, as was already evident from the differential event rates. Here we note that the maximum of the event rate happens at WIMP mass of roughly 30 GeV for elastic scattering and 50 GeV for inelastic scattering. This agrees with the analysis of the D_n nuclear structure coefficients. Adding a realistic detector threshold energy for nuclear recoils, the branching ratio to inelastic scattering would get more favorable, but not significantly so.

Due to the small inelastic scattering event rate for ^{83}Kr it is difficult to justify building a krypton detector. Moreover, the krypton used in such detector needs to be isotopically enriched in ^{83}Kr and the radioactive ^{85}Kr component needs to be minimized. Methods for the isotopic enrichment exist, but they are costly. Therefore, despite the interesting nuclear structure of ^{83}Kr, it is probably wiser to look for other targets.

In article [III] we performed similar calculations for event rates of WIMPs inelastically scattering off ^{125}Te. We used the same elementary WIMP-nucleon

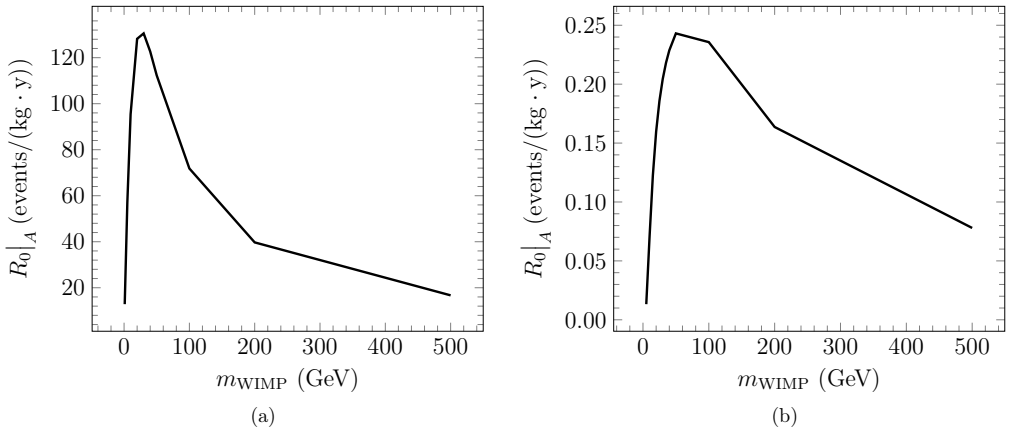

Figure 3.10. Time-averaged total event rate as a function of the WIMP mass for (a) elastic and (b) inelastic scattering off a ^{83}Kr target . Only spin-dependent scattering is included. The energy threshold used in the calculation was zero.

isovector cross section as in article [I], i.e., $\sigma_1(N) = 17\,\mathrm{fb}$. We also assumed a set of nonvanishing values for the isoscalar cross section for the calculation of total event rates.

The differential event rates with respect to recoil energy are given in Fig. 3.11 for (a) elastic scattering and (b) inelastic scattering. Results are shown for WIMP masses of 20, 50, 100, 200, 500, and 1000 GeV. The elastic scattering differential event rate is larger than that for ^{83}Kr at zero energy transfer, but it also falls faster with increasing E_{R}. The largest contribution to the elastic scattering event rate comes from small E_{R}, however. The difference in magnitude between the elastic and inelastic channel is not as large as for ^{83}Kr. Also for ^{125}Te the differential event rate extends to a wider range in E_{R}.

The time-averaged total event rate for ^{125}Te is given in Fig. 3.12 for (a) elastic scattering and (b) inelastic scattering. One immediately notices that the inelastic channel event rate is much higher than that of ^{83}Kr. Also the elastic channel event rate is sizable. The elastic scattering event rate peaks at $m_{\mathrm{WIMP}} \approx 30\,\mathrm{GeV}$ and the inelastic scattering event rate at $m_{\mathrm{WIMP}} \approx 200\,\mathrm{GeV}$. For a sufficiently heavy WIMP the branching ratio of inelastic to elastic scattering is not horribly suppressed.

The experimental feasibility of a Te detector is also discussed briefly in article [III]. To make the search of inelastic scattering events efficient, one would have to enrich the Te in the detector to a high percentage of ^{125}Te. A method to do this enrichment exists and while it has been utilized to enrich a sample to 93 % in ^{130}Te, the same could be done for ^{125}Te. The

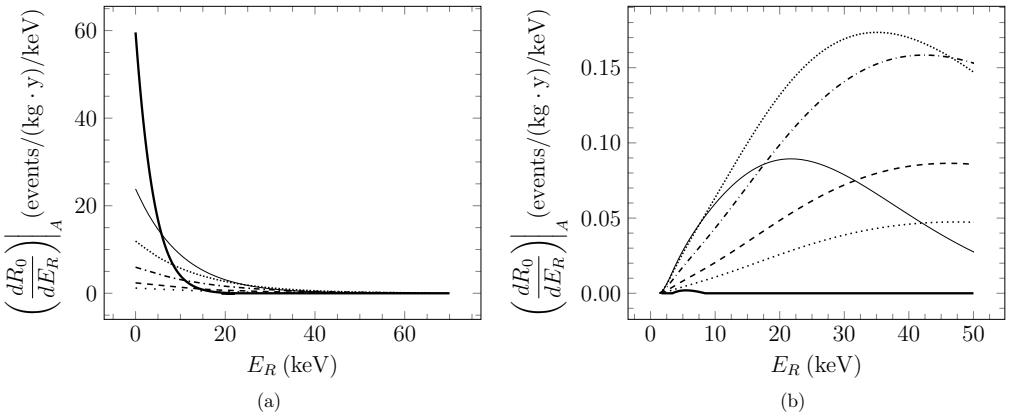

Figure 3.11. Differential event rate with respect to the nuclear recoil energy E_{R} for WIMPs of select masses scattering off a ^{125}Te target (a) elastically and (b) inelastically. Only spin-dependent scattering is included. The thick solid, solid, dotted, dashed-dotted, dashed, and loosely dotted lines correspond to WIMP masses of 20, 50, 100, 200, 500, and 1000 GeV, respectively.

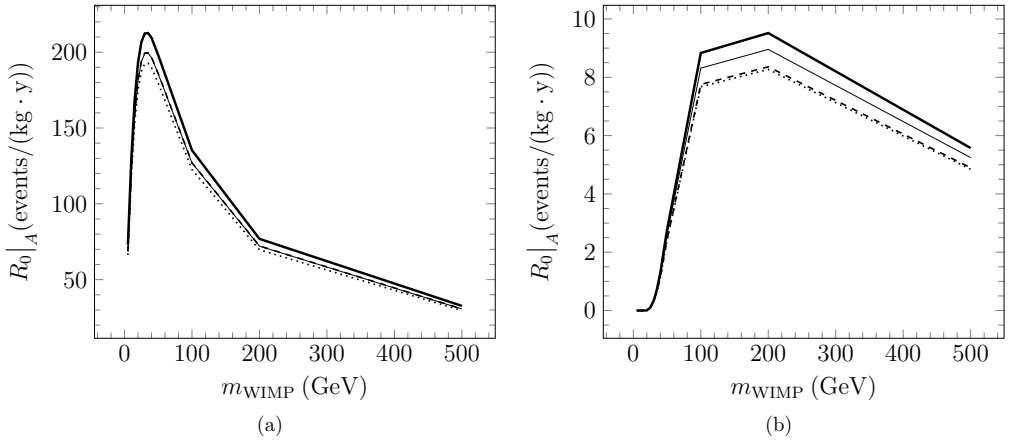

Figure 3.12. Time-averaged total event rate as a function of the WIMP mass for (a) elastic and (b) inelastic scattering off a ^{125}Te target. Only spin-dependent scattering is included. The thick solid, solid, dotted, and dashed curves correspond to $\sigma_0(N)/\sigma_1(N) = 0.014, 0.094, 0.41, 0.53$, respectively.

CUORE detector in Laboratori Nazionali del Gran Sasso operates a 740 kg total of TeO_2 bolometers, of which roughly 43 kg is ^{125}Te [111]. A search of inelastic WIMP-nucleus scattering events would be interesting already in CUORE data as we predict an event rate of $2.77, 2.61, 2.40, 2.43\,\mathrm{kg}^{-1}\mathrm{y}^{-1}$ for a 50 GeV WIMP and $8.88, 8.31, 7.67, 7.75\,\mathrm{kg}^{-1}\mathrm{y}^{-1}$ for a 100 GeV WIMP using $\sigma_0/\sigma_1 = 0.014, 0.094, 0.41, 0.53$, respectively. A CUORE-like detector enriched to over 90 % in ^{125}Te would be very interesting for inelastic WIMP-nucleus scattering searches. The detection signal in such detector would be a combined energy signal from the nuclear recoil and the de-excitation gamma ray. In principle one could notice the contribution of the inelastic scattering process in the total number of events as a rise in the measured energy spectrum at the experimental energy of the first excited state.

We have shown that a detector containing a large amount of ^{125}Te can open new opportunities for examining spin-dependent interactions of WIMPs with nuclei. However, this conclusion relies on several assumptions. To look for inelastic scattering events, the WIMP needs to be sufficiently heavy, as discussed above. Tellurium is quite rare and expensive, and to gather and enrich a large enough sample for a WIMP detector would be a massive investment. While the results of the present work would imply that a Te detector would optimally be more sensitive to spin-dependent interactions than a Xe detector, the theoretical uncertainties involved in the calculations make it difficult to draw certain conclusions on the matter. Therefore it is unlikely that a new ^{125}Te detector will be built to compete with the currently prevalent large-scale liquid xenon experiments.

Chapter 4

Neutrinos in dark-matter detectors

As has been discussed in the previous sections, the main mechanism of dark matter direct detection is detecting the recoil of a nucleus in an event of elastic coherent scattering with a dark matter particle. A problem with this approach emerges, when other particles scatter off the detector via a similar mechanism. Typical dark matter detectors are located deep underground, which helps to eliminate most backgrounds. However, the Earth is constantly bombarded with neutrinos from astrophysical sources which are impossible to shield against. It has recently been experimentally verified that neutrinos can scatter off nuclei coherently [107] and a sensitive enough detector is able to detect the small recoils caused by the light neutrinos.

A problem emerges in direct detection of dark matter when the detectors become sensitive enough to detect neutrinos. Nuclear recoils caused by neutrinos are difficult to distinguish from recoils caused by dark matter. While the event rate of neutrino events can be estimated, there is a sizable uncertainty in the event rate, and the dark matter event rate should be larger than that uncertainty to proclaim a detection. To make matters worse, the recoil spectra for WIMPs and neutrinos are predicted to be similar, especially for some specific WIMP masses [48]. This problem with the irreducible neutrino background is referred to as the neutrino floor in dark matter direct detection.

The neutrino floor is predicted to be reality for the next-generation dark matter detectors. It is therefore of paramount importance to find a way through the neutrino floor. While individual events may be indistinguishable, there might be some other experimental signals that can discriminate between neutrino and dark matter events. An annual modulation of the recoil event rate is expected for WIMPs, but the flux of most background neutrinos

should be roughly constant in time or have a different phase to the WIMP modulation. The different time signal of WIMPs and neutrinos in addition to the spectral data could possibly be used to solve the problem of the neutrino floor [112]. In an effective-field-theory approach some nonstandard operators have been shown to give a distinct recoil spectrum for WIMPs [113, 114]. Also directional information of the recoil signal could potentially be used as astrophysical neutrinos are coming from the direction of their source as opposed to WIMPs that are distributed in the dark-matter halo of the galaxy and are likely not coming collectively from a fixed direction [115, 116].

In this section we discuss the most prominent sources of neutrinos affecting dark matter detectors. We then outline the formalism for neutrino-nucleus scattering, and compute cross sections of ^{8}B solar neutrinos and supernova neutrinos scattering off the most abundant xenon isotopes. Both neutral-current and charged-current processes are investigated.

4.1 Background neutrino spectra

Let us look at the most prominent neutrino species to contribute to the neutrino floor. There are two things one must account for. Firstly, the neutrinos must have enough energy to give a detectable kick to the detector. For the next-generation xenon detectors, a reasonable lower limit for threshold energy is 1 keV. The maximum recoil energy for coherent elastic neutrino-nucleus scattering is [48]

$$E_{\mathrm{R,max}} = \frac{2E_\nu^2}{M + 2E_\nu}, \tag{4.1}$$

where E_ν is the neutrino energy and M is the mass of the nucleus. Therefore we can neglect all neutrino species with $E_{\mathrm{R,max}} \leq 1\,\mathrm{keV}$ for a given nucleus. Secondly, the flux of the neutrinos hitting the Earth has to be considered. Solar neutrinos have huge fluxes, but most types of solar neutrinos have too low energies. Atmospheric neutrinos have a wide energy spectrum, but the flux is several orders of magnitude lower than most of the solar neutrino sources [117]. The diffuse supernova background neutrinos can also be important, but their flux is also estimated to be low although the spectrum is not very well known [118]. Estimates of solar and atmospheric background neutrino spectra are shown in Fig. 4.1. Solar neutrino spectra for this work were read from the collection of Ref. [119]. The atmospheric neutrino spectrum in Fig. 4.1 is based on the highest flux evaluated in Ref. [117].

For a liquid Xe detector with mass number $A \approx 130$, Eq. (4.1) gives a minimum neutrino energy of roughly 7.8 MeV to have nuclear recoils of over

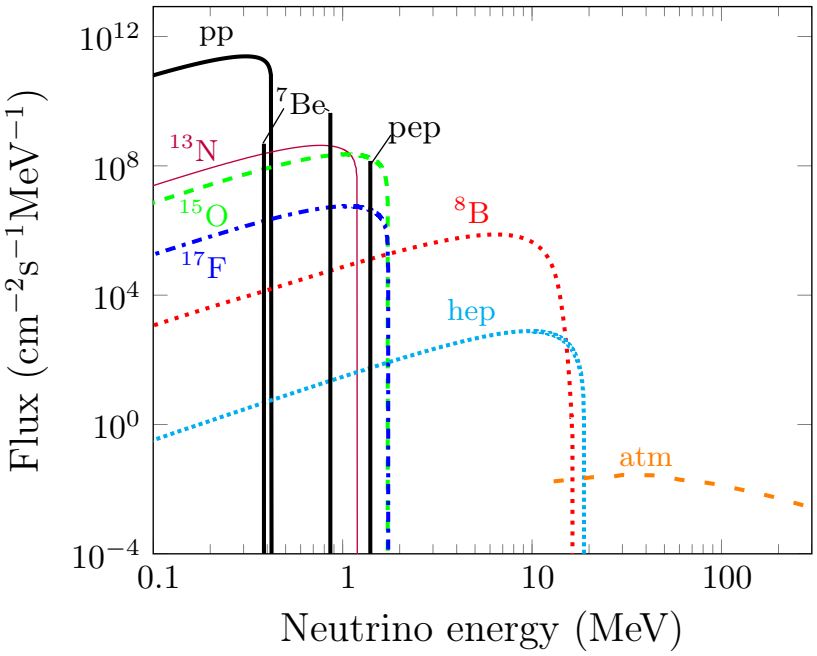

Figure 4.1. Estimates of the solar and atmospheric background neutrino spectra relevant for dark matter direct detection.

1 keV possible. The solar ^{8}B neutrinos seem to be in a sweet spot of having a decent portion of their energy spectrum in the desired energy range, but also have a high flux of roughly 5×10^{6} cm^{2}s^{-1} [120]. It is expected that the ^{8}B peak will be the first neutrinos detected by the dark matter experiments via a recoil signal [49, 50]. Therefore we have a focus on the ^{8}B neutrinos in our neutrino-nucleus scattering calculations.

Another interesting possibility is a supernova happening sufficiently close in our own galaxy. The neutrinos from a supernova arrive within a rather short time window, which does not make them a very problematic background over a long dark matter direct detection experiment, especially given timing information of scattering events, but such experiments could be able to probe into some new neutrino physics with the massive flux of energetic supernova neutrinos. It is noteworthy, that in principle the diffuse supernova background neutrinos can be detected in very sensitive detectors with long exposure, but that is out of scope for the next-generation detectors. For now we settle for investigating neutrinos from nearby observable supernovae.

The energy spectrum of supernova neutrinos can be modeled by using a two-parameter Fermi-Dirac distribution [121, 122]. The parameters entering the expression for the distribution are the neutrino temperature T_ν and the so-called pinching parameter α_ν. We can write the Fermi-Dirac distribution

as

$$f_{\rm FD}(E_{\mathbf{k}}) = \frac{1}{F_2(\alpha_\nu)T_\nu}\frac{(E_{\mathbf{k}}/T_\nu)^2}{1+e^{E_{\mathbf{k}}/T_\nu-\alpha_\nu}}, \tag{4.2}$$

where the normalization factor $F_2(\alpha_\nu)$ is given by

$$F_k(\alpha_\nu) = \int \frac{x^k dx}{1+e^{x-\alpha_\nu}}. \tag{4.3}$$

The temperature and mean energy $E_{\mathbf{k}}$ of neutrinos are equivalent in the sense that they are related by the expression

$$\frac{\langle E_\nu\rangle}{T_\nu} = \frac{F_3(\alpha_\nu)}{F_2(\alpha_\nu)}. \tag{4.4}$$

The plain Fermi-Dirac distribution for a given flavor of neutrinos can be altered significantly if neutrino mixing is present. In neutral-current processes this should not affect the total cross section if one sums over all neutrino flavors. However, in charged-current reactions only the electron neutrinos and antineutrinos can participate due to the high rest mass of the other charged leptons. As neutrinos are very likely to go through flavor conversions in the very dense supernova environment [123], this effect should be taken into account in the energy spectra for CC scattering. We follow the idea of Refs. [124, 125] that the mixing problem in supernovae can be reduced to a two-flavor mixing problem: $\nu_e \leftrightarrow \nu_x$, where ν_x is a linear combination of the muon and tau neutrinos.

As described above, the neutrino mixing induces changes to the bare Fermi-Dirac distribution given by Eq. (4.2). The modified energy profile for electron neutrinos can be given the form [126]

$$F_{\nu_{\rm e}} = p(E_{\mathbf{k}})F^0_{\nu_{\rm e}}(E_{\mathbf{k}}) + [1-p(E_{\mathbf{k}})]\,F^0_{\nu_x}(E_{\mathbf{k}}) \tag{4.5}$$

and for antineutrinos:

$$F_{\bar\nu_{\rm e}} = \bar p(E_{\mathbf{k}})F^0_{\bar\nu_{\rm e}}(E_{\mathbf{k}}) + [1-\bar p(E_{\mathbf{k}})]\,F^0_{\bar\nu_x}(E_{\mathbf{k}}). \tag{4.6}$$

Here $p(E_{\mathbf{k}})$ ($\bar p(E_{\mathbf{k}})$) denotes the neutrino (antineutrino) survival probability and $F^0_{\nu_l}(E_{\mathbf{k}})$ ($F^0_{\bar\nu_l}(E_{\mathbf{k}})$) is the bare Fermi-dirac energy distribution of neutrinos (antineutrinos).

The neutrino and antineutrino survival probabilities were read from Ref. [126]. In the case of normal neutrino mass hierarchy we have

$$p(E_{\mathbf{k}}) = 0, \tag{4.7}$$

and

$$\bar{p}(E_{\mathbf{k}}) = \begin{cases} \cos^2\theta_{12}, & \text{if } E_{\mathbf{k}} < \bar{E}_{\mathrm{s}}, \\ 0, & \text{if } E_{\mathbf{k}} \geq \bar{E}_{\mathrm{s}}, \end{cases} \tag{4.8}$$

where the split energy $\bar{E}_{\mathrm{s}}$ is taken to be 18 MeV following Ref. [127]. In the case of inverted mass hierarchy, the survival probabilities take the form

$$p(E_{\mathbf{k}}) = \begin{cases} \sin^2\theta_{12}, & \text{if } E_{\mathbf{k}} < E_{\mathrm{s}} \\ 0, & \text{if } E_{\mathbf{k}} \geq E_{\mathrm{s}} \end{cases} \tag{4.9}$$

and

$$\bar{p}(E_{\mathbf{k}}) = \cos^2\theta_{12}, \tag{4.10}$$

where we use the value $E_{\mathrm{s}} = 7$ MeV read from Ref. [124], and $\sin^2\theta_{12} = 0.306\ (0.312)$ for normal (inverted) neutrino mass hierarchy [128].

4.2 Neutrino-nucleus scattering

A neutrino can scatter off an atomic nucleus via an exchange of a neutral Z boson or a charged W boson. These scattering processes are referred to as neutral-current (NC) and charged-current (CC) channels, respectively. Neutral-current processes can be written as

$$\nu_l + (A, Z) \to \nu_l' + (A, Z), \tag{4.11}$$
$$\nu_l + (A, Z) \to \nu_l' + (A, Z)^*, \tag{4.12}$$

where proton number Z does not change between the initial and final nuclear state. We label the lepton flavor of the involved neutrino by $l = \mathrm{e}, \mu, \tau$, and the same expressions are valid also for antineutrinos $\bar{\nu}_l$. The scattering process can be elastic as in Eq. (4.11), i.e., the nucleus remains in its initial state and only receives kinetic recoil energy from the neutrino. In inelastic scattering, Eq. (4.12), in addition to a recoil energy the nucleus is excited to a higher energy level. Charged-current processes change the charge of the nucleus and can be written as

$$\nu_l + (A, Z) \to l^- + (A, Z+1)^*, \tag{4.13}$$
$$\bar{\nu}_l + (A, Z) \to l^+ + (A, Z-1)^*, \tag{4.14}$$

where the final state nucleus is usually in some excited state. The NC and CC scattering processes and kinematics involved are illustrated in Fig. 4.2. In the figure and in the following discussion we will refer to the four-momenta

of the incoming and outgoing leptons as k_μ and k'_μ. Incoming and outgoing lepton energies are labeled as E_k and $E_{k'}$. The momentum transferred to the nucleus is $q_\mu = k'_\mu - k_\mu = p_\mu - p'_\mu$, where p_μ and p'_μ are the initial and final state momenta of the nucleus.

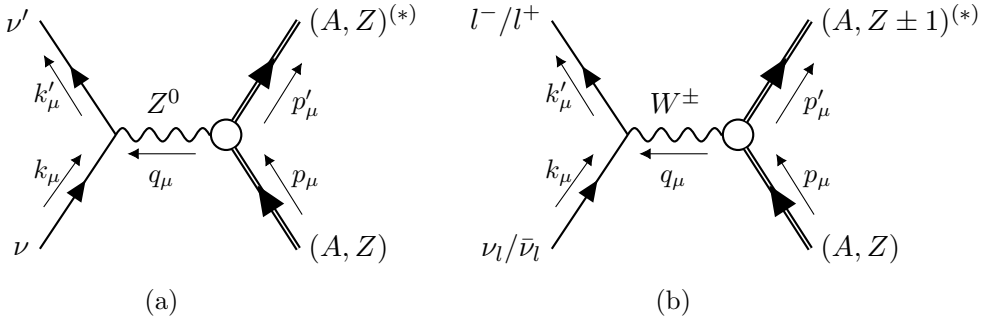

Figure 4.2. Diagram of (a) neutral-current and (b) charged-current scattering of a neutrino off a nucleus with mass number A and proton number Z.

The differential cross section for neutral-current scattering to a final state of energy E_{exc} is [53]

$$\frac{d^2\sigma}{d\Omega dE_{\text{exc}}} = \frac{G_{\text{F}}^2 \left|\mathbf{k}'\right| E_{k'}}{\pi(2J_i+1)} \left(\sum_{J\geq 0} \sigma_{\text{CL}}^J + \sum_{J\geq 1} \sigma_{\text{T}}^J \right), \tag{4.15}$$

where G_{F} is the Fermi coupling constant and J_i is the angular momentum of the initial nuclear state. The cross section for charged-current scattering looks similar, but has a few added ingredients [54, 129]:

$$\frac{d^2\sigma}{d\Omega dE_{\text{exc}}} = \frac{G_{\text{F}}^2 \cos^2\theta_{\text{C}} \left|\mathbf{k}'\right| E_{k'}}{\pi(2J_i+1)} F(\pm Z_f, E_{\mathbf{k}'}) \left(\sum_{J\geq 0} \sigma_{\text{CL}}^J + \sum_{J\geq 1} \sigma_{\text{T}}^J \right), \tag{4.16}$$

where $F(\pm Z, E_{\mathbf{k}'})$ is a Fermi function and θ_{C} is the Cabibbo angle. The Fermi function is used only for relatively low effective momenta, while the modified effective momentum approach of Ref. [130] is followed to correctly treat the final-state interactions for higher effective momenta.

The Coulomb-longitudinal (σ_{CL}^J) and transverse (σ_{T}^J) parts of the cross-section formulas (4.15) and (4.16) are defined as

$$\begin{aligned}\sigma_{\text{CL}}^J =& (1 + a\cos\theta) \left|\langle J_f||\mathcal{M}_J(q)||J_i\rangle\right|^2 + (1 + a\cos\theta - 2b\sin^2\theta) \left|\langle J_f||\mathcal{L}_J(q)||J_i\rangle\right|^2 \\ &+ \frac{E_{\mathbf{k}} - E_{\mathbf{k}'}}{q}(1 + a\cos\theta + c) \times 2\text{Re}\left\{\langle J_f||\mathcal{M}_J(q)||J_i\rangle^* \langle J_f||\mathcal{L}_J(q)||J_i\rangle\right\},\end{aligned} \tag{4.17}$$

and

$$\sigma_{\mathrm{T}}^{J} = \left(1 - a\cos\theta + b\sin^2\theta\right)\left[\left|\langle J_f||\mathcal{T}_J^{\mathrm{mag}}(q)||J_i\rangle\right|^2 + \left|\langle J_f||\mathcal{T}_J^{\mathrm{el}}(q)||J_i\rangle\right|^2\right] \mp \frac{E_{\mathbf{k}} + E_{\mathbf{k}'}}{q}(1 - a\cos\theta - c) \times 2\mathrm{Re}\left\{\langle J_f||\mathcal{T}_J^{\mathrm{mag}}(q)||J_i\rangle\langle J_f||\mathcal{T}_J^{\mathrm{el}}||J_i\rangle^*\right\}, \tag{4.18}$$

where θ is the scattering angle, the minus (plus) sign is taken for neutrinos (antineutrinos), and

$$a = \sqrt{1 - (m_l/E_{\mathbf{k}'})^2}, \tag{4.19}$$

$$b = \frac{a^2 E_{\mathbf{k}} E_{\mathbf{k}'}}{q^2}, \tag{4.20}$$

and

$$c = \frac{m_l^2}{q E_{\mathbf{k}'}}. \tag{4.21}$$

It is noteworthy that for NC scattering $a = 1$ and c vanishes as the final-state lepton mass m_l is just the very small neutrino mass, taken to be zero in this work. The operators $\mathcal{M}_{JM}(q)$, $\mathcal{L}_{JM}(q)$, $\mathcal{T}_{JM}^{\mathrm{mag}}(q)$, and $\mathcal{T}_J^{\mathrm{el}}(q)$ appearing in Eqs. (4.17) and (4.18) correspond to the Coulomb, longitudinal, transverse magnetic, and transverse electric multipole operators, respectively. We assume that the impulse approximation holds, and we consider these operators as one-body operators. However, it should be noted that two-body currents might also be of some importance in neutrino-nucleus scattering.

Here we have presented the most essential ingredients entering the neutrino-nucleus scattering cross section. The formalism and the various operators included in the σ_{CL}^{J} and σ_{T}^{J} parts are described in further detail in Refs. [55, 129, 131, 132].

4.3 Results

Motivated by the neutrino-floor problem in large-scale xenon dark-matter detectors, we have computed cross sections for neutral-current and charged-current neutrino-nucleus scattering processes off the most abundant Xe isotopes. We have made calculations for solar ^{8}B neutrinos using the energy spectrum of Ref. [133]. For supernova neutrinos we have used a Fermi-Dirac distribution with the parameters $\langle E_{\mathbf{k}}\rangle$, T_ν, and α_ν listed in Table 4.1 for electron (ν_e) and muon/tau (ν_x) neutrinos and the corresponding antineutrinos.

Table 4.1. The values of the parameters entering the Fermi-Dirac distribution, i.e., the pinching parameter α_ν (column 3), the average neutrino energy $\langle E_\mathbf{k} \rangle$ (column 4), and neutrino temperature T_ν (column 5). Note that different values of α_ν were used for neutral-current and charged-current scattering for muon/tau neutrinos. Parameter values are given for electron and muon/tau (anti)neutrinos ν_e, ν_x ($\bar{\nu}_e, \bar{\nu}_x$) specified in column 2. The parameter sets were taken from Ref. [83] for NC scattering and in Ref. [58] for CC scattering.

Scattering	Flavor	α_ν	$\langle E_\mathbf{k} \rangle$ (MeV)	T_ν (MeV)
NC	ν_e	3.0	11.5	2.88
	$\bar{\nu}_e$	3.0	13.6	3.41
	ν_x	3.0	16.3	5.17
	$\bar{\nu}_x$	3.0	16.3	5.17
CC	ν_e	3.0	11.5	2.88
	$\bar{\nu}_e$	3.0	13.6	3.41
	ν_x	0.0	16.3	5.17
	$\bar{\nu}_x$	0.0	16.3	5.17

4.3.1 Neutral-current processes

In article [IV] we computed cross sections for NC neutrino-nucleus scattering off ^{128}Xe, ^{129}Xe, ^{130}Xe, ^{131}Xe, ^{132}Xe, ^{134}Xe, and ^{136}Xe. We performed the nuclear structure calculations in the QRPA for both coherent elastic scattering and incoherent inelastic scattering off even-mass isotopes. For the odd-mass isotopes the MQPM was used. A shell-model calculation was also used to compute the coherent scattering cross sections for comparison, but the differences to the QRPA/MQPM results were appreciably small. Here we therefore only highlight results computed in the quasiparticle schemes.

The total averaged cross sections for the target xenon isotopes are shown in Fig. 4.3 for coherent elastic scattering (panel (a)) and inelastic scattering (panel (b)). The cross sections for coherent scattering are sensitive to the neutrino energy, but not as much as the inelastic scattering cross sections. The inelastic scattering cross sections for ^{8}B and ν_x supernova neutrinos differ by two orders of magnitude. Our total averaged cross sections for the Xe isotopes are very similar to those obtained for Cd isotopes in [51]. There does not seem to be a nuclear structure effect favoring either Xe or Cd over the other as a neutrino detector.

We present the contributions to the total inelastic scattering cross section arising from different multipole channels for solar ^{8}B neutrinos and supernova electron neutrinos in Fig. 4.4. The results are shown for the even-mass

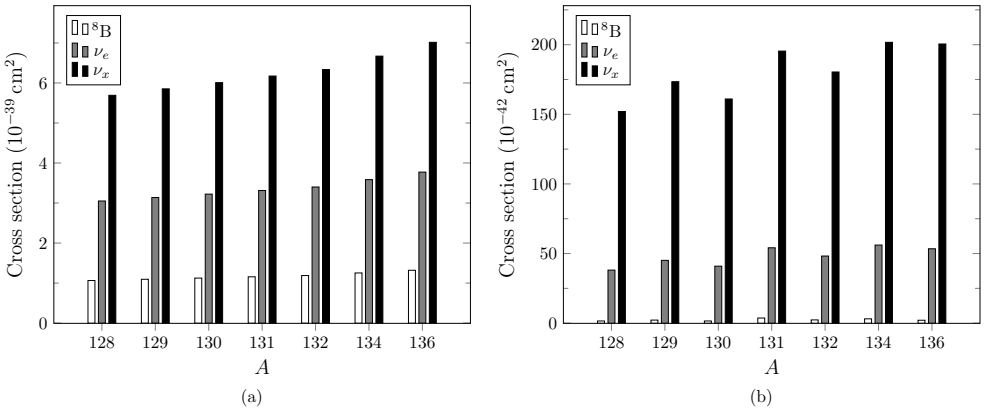

Figure 4.3. The total averaged cross sections of neutrinos scattering via neutral current (a) coherently and (b) inelastically off the target Xe isotopes. Values for ^{8}B neutrinos, supernova electron neutrinos and supernova muon/tau neutrinos are shown in the figure.

^{128}Xe and the odd-mass ^{129}Xe. The leading contribution to NC scattering is expected to come from the 1^+ axial-vector channel, although especially for the odd-mass isotopes we found large contributions from the vector 0^+ multipole channel. One question raised in this work is, whether the MQPM approach to the cross-section calculations overestimates the contribution of the 0^+ multipole. This behavior has been noticed before in Ref. [51] for odd-mass Cd isotopes. The 0^+ multipole should vanish at the limit of zero momentum transfer, and therefore the contribution should be small barring very large neutrino energies. Hence the total cross sections for odd-mass nuclei were concluded to probably be somewhat overestimated by spurious contributions from the 0^+ multipole. Up to date we have not discovered any concrete reason for the overestimation, but it might have something to do with the violated particle number in the quasiparticle scheme.

We also investigated the contributions coming from different final states in the excited nucleus. In even-mass Xe isotopes the scattering process seems to favor high-lying 1^+ states around 5 to 8 MeV. A low-lying 0^+ state often contributes notably to the cross section for the lower-energy solar neutrinos but to much lesser extent for supernova neutrinos. In odd-mass nuclei we found a bunch of states around 8 MeV giving a large contribution to supernova neutrino cross sections, but for the lower energy ^{8}B neutrinos they had a much smaller effect in the total cross section.

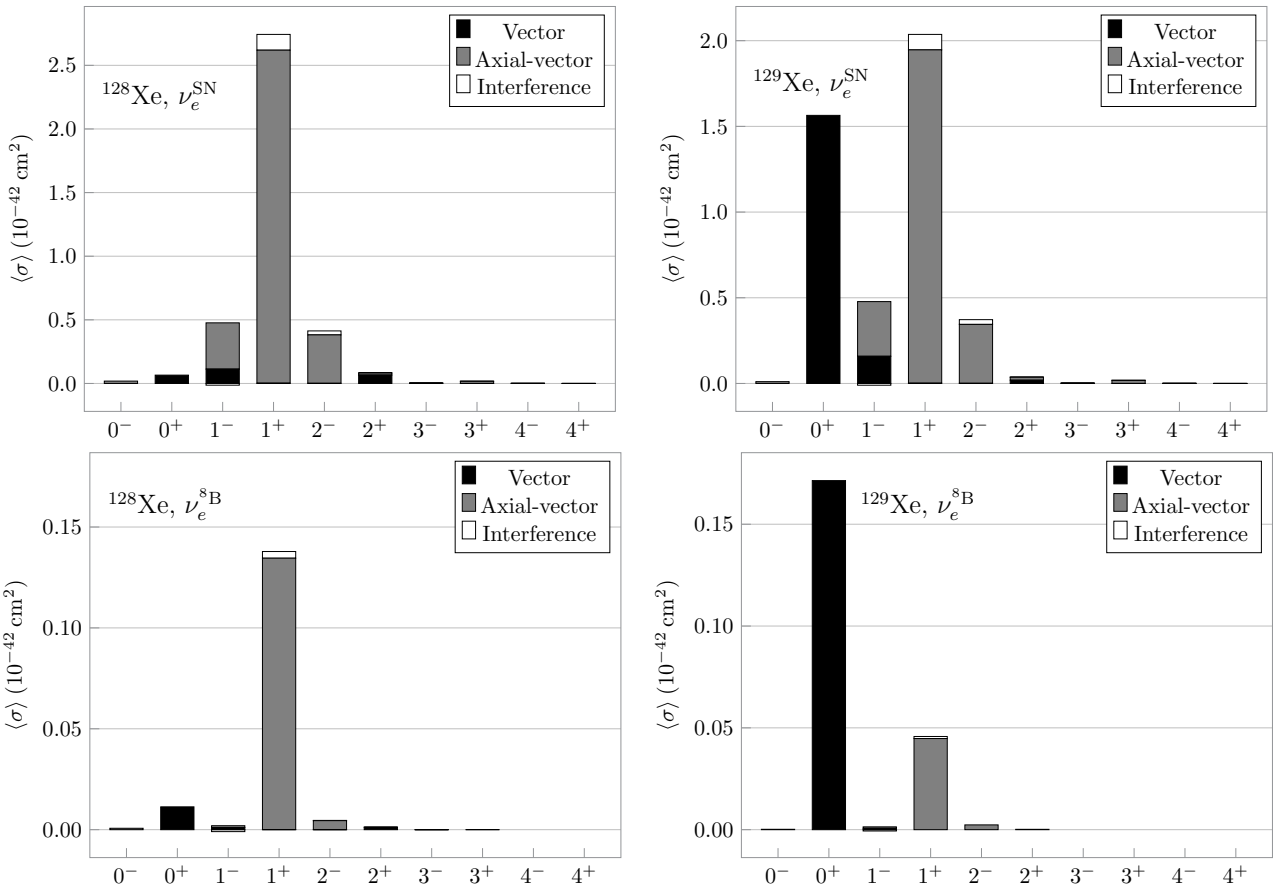

Figure 4.4. Contributions to the total averaged cross section of inelastic scattering of supernova electron neutrinos (top row) and solar ^{8}B neutrinos (bottom row) off a representative sample of one even-mass and one odd-mass xenon target. The results are shown for ^{128}Xe (left column) and ^{129}Xe (right column). The contributions from the vector, axial-vector, and interference parts of the interaction are also shown. Cross sections are given in units of 10^{-42} cm^2.

4.3.2 Charged-current processes

The charged-current processes based on the same Xe targets were studied in article [V]. Here we computed the wave functions of the involved states in the pnQRPA formalism for the even-mass nuclei, and MQPM for the odd-mass nuclei.

We found that Gamow-Teller giant resonance (GTGR) states are very important in the CC processes ${}^{A}\mathrm{Xe} + \nu_e \rightarrow {}^{A}\mathrm{Cs} + e^-$ for even-mass Xe targets. This has a hindering effect for the solar ${}^{8}\mathrm{B}$ neutrinos, as only the very tail of the energy spectrum is able to excite the transition to the GTGR. The 0^+ isobaric analog state (IAS) is also important in all cases, but often to a lesser extent than the GTGR. The energy of the IAS is often underestimated in a pnQRPA calculation [134]. In this work we have set the energy of the IAS to match a prediction of an empirical formula presented in Ref. [135]. When the energy of the IAS is corrected, its contribution to the cross section decreases to a reasonable level, yet it remains significant.

We notice a very strong odd-even effect in the total averaged cross sections for both neutrinos and antineutrinos. The total cross sections of supernova electron neutrinos and antineutrinos scattering off the various Xe targets are presented in Fig. 4.5 in panel (a) and (b), respectively. The effects of neutrino mixing are not yet included. We notice a roughly four-fold increase in the cross sections for ${}^{129}\mathrm{Xe}$ and ${}^{131}\mathrm{Xe}$ compared to their even-mass neighbors. Interestingly enough, while we discussed a spurious large contribution from the 0^+ multipole in NC reactions, such anomaly does not seem to be present in our CC calculations. Partly the larger cross sections for the odd-mass targets can be explained by the smaller Q value of the reaction.

We then include the neutrino flavor conversions into the mix, and the resulting cross sections are shown in Fig. 4.6. The main result here is that while the cross sections for neutrinos remain similar regardless whether the neutrinos have normal or inverted mass hierarchy, the situation is very different for antineutrinos. For antineutrinos scattering off a Xe target, the cross sections differ by roughly a factor of two between normal and inverted hierarchies. Therefore the neutrino mass hierarchy could in principle be determined by observing supernova antineutrinos in a detector. A similar observation has been made in Refs. [52] and [57] for Cd and Ar targets, respectively. Limiting factors to this are the sensitivity of the detector, the uncertainty of the theoretical prediction, and uncertainties of the neutrino energy distribution. The effect is slightly dependent on the parameters chosen for the Fermi-Dirac distribution. Therefore calculations with a wide range of Fermi-Dirac parameters, more elaborate model for neutrino mixing, and perhaps also with a range of different nuclear models should be made to make

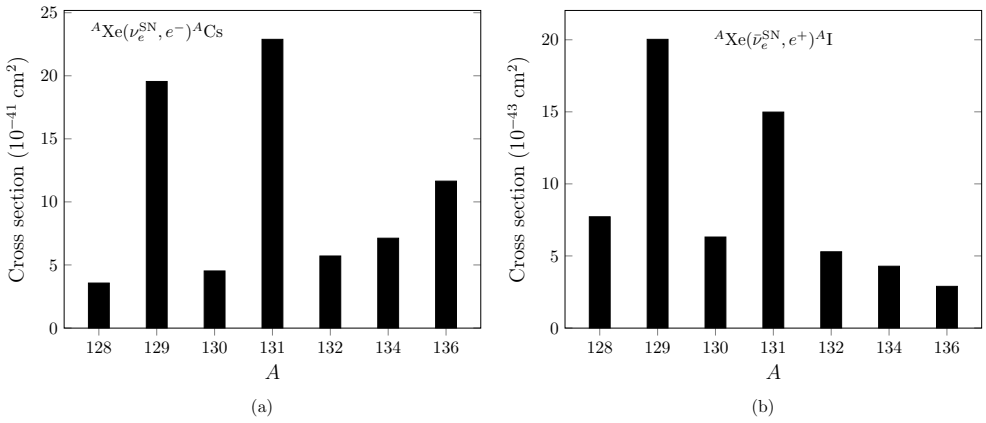

Figure 4.5. The total averaged cross sections of charged-current scattering of (a) neutrinos and (b) antineutrinos off the target Xe isotopes. Neutrino mixing has not been accounted for. Note the different units on the y-axes of the two panels.

more reliable conclusions on the feasibility of this strategy.

The contribution of different multipole operators to the total cross sections of CC scattering are shown in Fig. 4.7 for ^{128}Xe and ^{129}Xe targets. Results are shown for energy spectra of supernova electron neutrinos, solar ^{8}B neutrinos and supernova electron antineutrinos. In our results for even-mass targets the most important multipole for neutrino scattering is 1^+. There are some smaller contributions to the cross section from the 0^+ and 2^- multipoles. Smaller neutrino energy appears to favor the 1^+ axial vector channel. The behavior is rather similar for both even-mass and odd-mass isotopes. For antineutrinos the situation is different. For even-mass nuclei the dominant multipole is 1^- with a mix of vector and axial-vector contributions. Also 1^+ and 2^- multipoles give a sizable contribution to the cross section. For odd-mass nuclei the contributions between 1^- and 1^+ are almost equal.

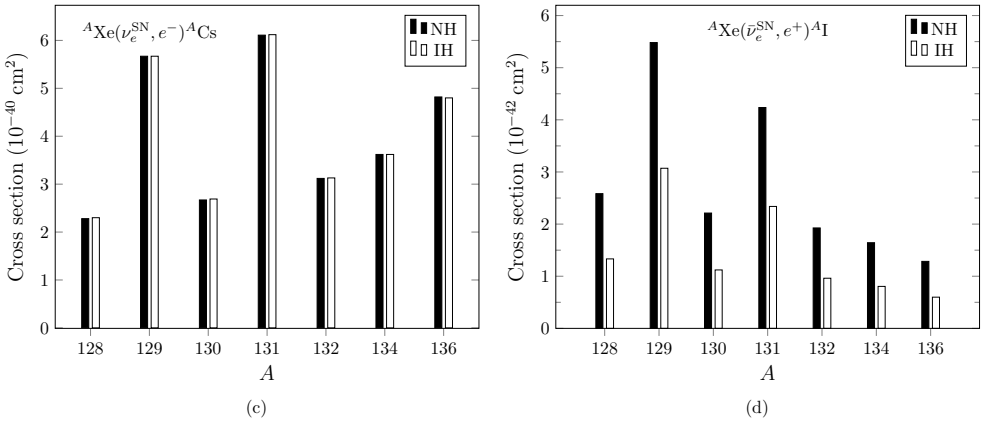

Figure 4.6. The total averaged cross sections of charged-current scattering of (a) neutrinos and (b) antineutrinos off the target Xe isotopes. Neutrino mixing has been accounted for and results are shown for the normal (NH) and inverted (IH) neutrino mass hierarchies in the black and white columns, respectively. Note the different units on the y-axes of the two panels.

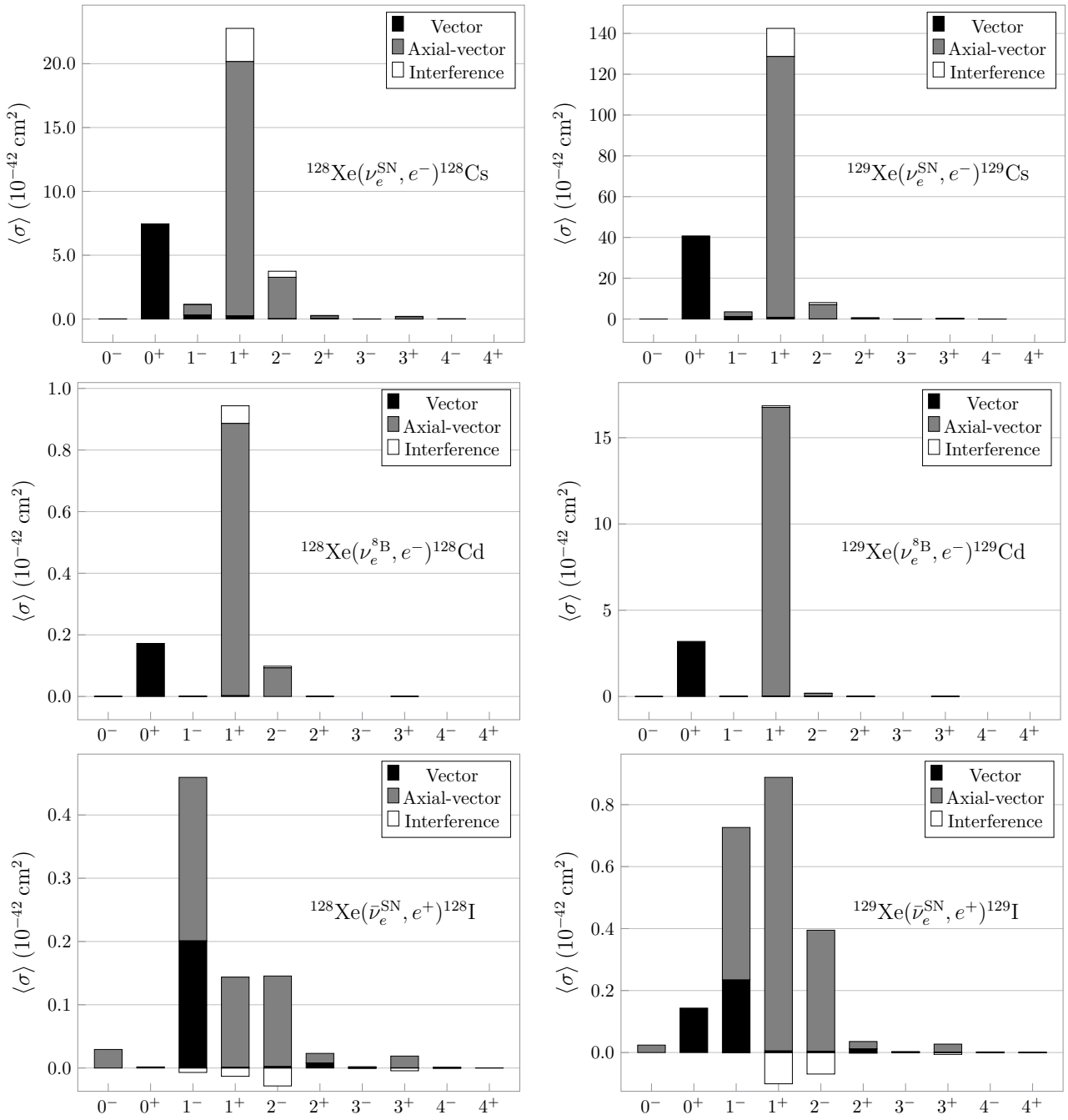

Figure 4.7. Contributions to the total averaged cross section of charged-current scattering of supernova electron neutrinos (top row), solar ^{8}B neutrinos (middle row), and supernova electron antineutrinos (bottom row) off a representative sample of one even-mass and one odd-mass xenon target. The results are shown for ^{128}Xe (left column) and ^{129}Xe (right column). The contributions from the vector, axial-vector, and interference parts of the interaction are also shown. Cross sections are given in units of $10^{-42}\,\mathrm{cm}^2$.

Chapter 5

Summary, conclusions, and outlook

In this thesis we have examined new candidate nuclei for WIMP direct detection, namely ^{83}Kr and ^{125}Te. We have especially focused on spin-dependent WIMP-nucleus interactions. We have also computed neutrino-nucleus scattering cross sections for ^{8}B neutrinos and supernova neutrinos scattering off Xe targets, motivated by the problem of neutrino floor in direct detection experiments and the neutrino-physics potential of the next-generation dark matter detectors.

In article [II] we examine the nuclear structure of ^{83}Kr and ^{125}Te and look how the nuclear structure affects WIMP-nucleus scattering. The nuclear-structure calculations were performed in the framework of the nuclear shell model. While the kinematic advantages provided by ^{83}Kr for inelastic scattering initially seemed promising, it became evident in our calculations that utilizing ^{83}Kr in a detector would be somewhat unreasonable, as more suitable candidates exist. We show that ^{125}Te is one such candidate. The nuclear structure of ^{125}Te appears to be very favorable for spin-dependent interactions compared to other targets for which similar calculations have been performed, such as ^{127}I, ^{129,131}Xe, and ^{133}Cs.

The conclusions of article [II] are supported by the event-rate estimations made in articles [I] and [III] for ^{83}Kr and ^{125}Te, respectively. In these articles we also examine the experimental feasibility of each potential new target. In addition to the small expected event rates for ^{83}Kr, it would be quite difficult (although possible) to build a sensitive detector utilizing a Kr target. For Te on the other hand, the CUORE collaboration has already demonstrated a working TeO_2 bolometer. A similar detector enriched to higher concentrations of ^{125}Te would be a very sensitive probe of spin-dependent interactions between WIMPs and nuclei. That being said, such detector would be very costly,

and further feasibility studies are required to justify building one. In the meantime, it might already be interesting to look for inelastic scattering events in the data of the currently running CUORE experiment.

In articles [IV] and [V] we present computed cross sections of neutral-current and charged-current scattering of neutrinos off the most abundant Xe isotopes ($A = 128$,129, 130,131, 132,134, 136). The wave functions of the involved even-even, odd-odd, and even-odd nuclei were computed in the QRPA, pnQRPA, and MQPM frameworks, respectively. Our calculations present the first estimates of the cross sections computed in a complete microscopic framework for isotopes other than ^{132}Xe (CC) and ^{136}Xe (NC and CC), and our results show improvement upon the earlier results for both cases.

We computed cross sections as a function of the energy of the incoming neutrino, but we also estimated cross sections for the ^{8}B solar neutrino energy spectrum and a Fermi-Dirac distribution was used to estimate cross sections for typical supernova (anti)neutrinos. For the even-mass isotopes our cross-section predictions are expected to be fairly accurate. For the odd-mass isotopes an unexpectedly large 0^+ multipole contribution was observed in the neutral-current case. This is possibly due to the particle-number violation in the quasiparticle scheme, but further investigation is required to solve the origin of the issue. Therefore, the computed cross-sections for NC scattering off ^{129}Xe and ^{131}Xe are probably somewhat overestimated.

In CC scattering of supernova neutrinos off even-mass xenon nuclei the high-lying Gamow-Teller giant resonance state and the isobaric analog state were very important in terms of total cross section. For the less energetic ^{8}B solar neutrinos the resonance states cannot be populated as strongly. This gives a relative enhancement to the scattering event rate off odd-mass nuclei where the most important final states were predicted to be at lower energies. Also in presence of neutrino mixing, the cross sections of supernova-antineutrinos scattering off xenon nuclei were predicted to be sensitive to the neutrino mass hierarchy for the model used in this work. The result appears to be somewhat model dependent, however, and further examination needs to be done to draw more confident conclusions.

Bibliography

[I] J. D. Vergados, F. T. Avignone III, P. Pirinen, P. C. Srivastava, M. Kortelainen, and J. Suhonen, *Phys. Rev. D* **92**, 015015 (2015).

[II] P. Pirinen, P. C. Srivastava, J. Suhonen, and M. Kortelainen, *Phys. Rev. D* **93**, 095012 (2016).

[III] J. D. Vergados, F. T. Avignone III, M. Kortelainen, P. Pirinen, P. C. Srivastava, J. Suhonen, A. W. Thomas, *J. Phys. G: Nucl. Part. Phys.* **43**, 115002 (2016).

[IV] P. Pirinen, J. Suhonen, and E. Ydrefors, *Adv. High Energy Phys.* **2018**, 9163586 (2018).

[V] P. Pirinen, J. Suhonen, and E. Ydrefors, "Charged-current neutrino-nucleus scattering off Xe isotopes", submitted to Phys. Rev. C (2018).

[6] F. Zwicky, *Helv. Phys. Acta* **6**, 110–127 (1933).

[7] V. C. Rubin and W. K. Ford, Jr., *Astrophys. J.* **159**, 379–403 (1970).

[8] J. Einasto, A. Kaasik, and E. Saar, *Nature* **250**, 309–310 (1974).

[9] M. S. Roberts and R. N. Whitehurst, *Astrophys. J.* **201**, 327–346 (1975).

[10] G. R. Blumenthal, S. M. Faber, J. R. Primack, and M. J. Rees, *Nature* **311**, 517–525 (1974).

[11] M. Davis, G. Efstathiou, C. S. Frenk, and S. D. M. White, *Astrophys. J.* **292**, 371–394 (1975).

[12] G. Hinshaw *et al.*, *Astrophys. J. Suppl. Ser.* **208**, 19 (2013).

[13] The Planck collaboration, P. A. R. Ade *et al.*, *Astron. Astrophys.* **571** A16 (2014).

[14] H. C. Cheng, J. L. Feng, K. T. Matchev, *Phys. Rev. Lett.* **89**, 211301 (2002).

[15] V. K. Oikonomou, J. D. Vergados, and Ch. C. Moustakidis, *Nucl. Phys. B* **773**, 19–42 (2007).

[16] S. Nussinov, *Phys. Lett. B* **165**, 55–58 (1985)

[17] S. B. Gudnason, C. Kouvaris, and F. Sannino, *Phys. Rev. D* **74**, 095008 (2006).

[18] J. Hubisz, and P. Meade, *Phys. Rev. D* **71**, 035016 (2005).

[19] A. Birkedal, A. Noble, M. Perelstein, and A. Spray, *Phys. Rev. D* **74**, 035002 (2006).

[20] G. Jungman, M. Kamionkowski, K. Griest, *Phys. Rep.* **267**, 195–373 (1996).

[21] J. Engel, S. Pittel, and P. Vogel, *Int. J. Mod. Phys. E* **1**, 1 (1992).

[22] C. Amole *et al.* (the PICO collaboration), *Phys. Rev. Lett.* **118**, 251301 (2017).

[23] R. Bernabei *et al.*, arXiv:1805.10486 [hep-ex] (2018).

[24] G. Adhikari *et al.*, *Eur. Phys. J. C* **78**, 107 (2018).

[25] H. S. Lee on behalf of the KIMS collaboration, *Nuclear and Particle Physics Proceedings* **273–275**, 295–301 (2016).

[26] R. Agnese *et al.* (SuperCDMS collaboration), *Phys. Rev. D* **95**, 082002 (2017).

[27] E. Armengaud *et al.*, *JCAP* **05**, 019 (2016).

[28] E. Aprile *et al.* (XENON collaboration), *Phys. Rev. Lett.* **119**, 181301 (2017).

[29] K. Abe *et al.* (XMASS collaboration), *Phys. Lett. B* **759**, 272–276 (2016).

[30] D. S. Akerib *et al.*, arXiv:1802.06039 [astro-ph.IM] (2018).

[31] X. Cui *et al.* (PandaX-II Collaboration), *Phys. Rev. Lett.* **119**, 181302 (2017).

[32] J. Ellis, R. A. Flores, J. D. Lewin, *Phys. Lett. B* **212**, 375–380 (1988).

[33] J. Ellis, and R. A. Flores, *Nucl. Phys. B* **307**, 883–908 (1988).

[34] J. Engel, and P. Vogel, *Phys. Rev. D* **40**, 3132 (1989).

[35] F. Iachello, and L. M. Krauss, *Phys. Lett. B* **254**, 220–224 (1991).

[36] E. Holmlund, M. Kortelainen, T. S. Kosmas, J. Suhonen, and J. Toivanen, *Phys. Lett. B* **584**, 31–39 (2004).

[37] M. T. Ressell, M. B. Aufderheide, S. D. Bloom, K. Griest, G. J. Mathews, and D. A. Resler, *Phys. Rev. D* **48**, 5519 (1993).

[38] P. C. Divari, T. S. Kosmas, J. D. Vergados, and L. D. Skouras, *Phys. Rev. C* **61**, 054612 (2000).

[39] M. Kortelainen, T. S. Kosmas, J. Suhonen, and J. Toivanen, *Phys. Lett. B* **632**, 226–232 (2006).

[40] P. Toivanen, M. Kortelainen, J. Suhonen, and J. Toivanen, *Phys. Rev. C* **79**, 044302 (2009).

[41] J. Menéndez, D. Gazit, and A. Schwenk, *Phys. Rev. D* **86**, 103511 (2012).

[42] L. Baudis, G. Kessler, P. Klos, R. F. Lang, J. Menéndez, S. Reichard, and A. Schwenk, *Phys. Rev. D* **88**, 115014 (2013).

[43] L. Vietze, P. Klos, J. Menéndez, W. C. Haxton, and A. Schwenk, *Phys. Rev. D* **91**, 043520 (2015).

[44] P. Klos, J. Menéndez, D. Gazit, and A. Schwenk, *Phys. Rev. D* **88**, 083516 (2013).

[45] M. T. Ressell, and D. J. Dean, *Phys. Rev. C* **56**, 535–546 (1997).

[46] A. L. Fitzpatrick, W. Haxton, E. Katz, N. Lubbers, and Y. Xu, *JCAP* **02**, 004 (2013)

[47] N. Anand, A. L. Fitzpatrick, and W. C. Haxton, *Phys. Rev. C* **89**, 065501 (2014).

[48] J. Billard and E. Figueroa-Feliciano, *Phys. Rev. D* **89**, 023524 (2014).

[49] J. D. Vergados and H. Ejiri, *Nucl. Phys. B* **804** 144–159 (2008).

[50] L. E. Strigari, *New J. Phys.* **11** 105011 (2009).

[51] W. Almosly, E. Ydrefors, and J. Suhonen, *J. Phys. G: Nucl. Part. Phys.* **42**, 025106 (2015).

[52] W. Almosly, E. Ydrefors, and J. Suhonen, *J. Phys. G: Nucl. Part. Phys.* **42**, 095106 (2015).

[53] E. Ydrefors, K. G. Balasi, J. Suhonen, T. S. Kosmas: Nuclear Responses to Supernova Neutrinos for the Stable Molybdenum Isotopes, In: *Neutrinos: Properties, Sources and Detection*, Physics Research and Technology, (Nova Science Publishers, 2011).

[54] E. Ydrefors, K. G. Balasi, T. S. Kosmas, and J. Suhonen, *Nucl. Phys. A* **896**, 1–23 (2012).

[55] E. Ydrefors and J. Suhonen, *Adv. High Energy Phys.* **2012**, 373946 (2012).

[56] W. Almosly, B. G. Carlsson, J. Suhonen, J. Toivanen, and E. Ydrefors, *Phys. Rev. C* **94**, 044614 (2016).

[57] J. Kostensalo, J. Suhonen, and K. Zuber, *Phys. Rev. C* **97**, 034309 (2018).

[58] E. Ydrefors, J. Suhonen, and Y. M. Zhao, *Phys. Rev. C* **91**, 014307 (2015).

[59] P. C. Divari, *Adv. High Energy Phys.* **2013**, 143184 (2013).

[60] T. Suzuki, S. Chiba, T. Yoshida, T. Kajino, and T. Otsuka, *Phys. Rev. C* **74**, 034307 (2006).

[61] C. Volpe, N. Auerbach, G. Colò, T. Suzuki, and N. Van Giai, *Phys. Rev. C* **62**, 015501 (2000).

[62] W. C. Haxton, *Phys. Rev. D* **36**, 2283 (1987).

[63] W. E. Ormand, P. M. Pizzochero, P. F. Bortignon, and R. A. Broglia, *Phys. Lett. B* **345**, 343–350 (1995).

[64] T. Suzuki, M. Honma, K. Higashiyama, T. Yoshida, T. Kajino, T. Otsuka, H. Umeda, and K. Nomoto, *Phys. Rev. C* **79**, 061603(R) (2009).

[65] R. Lazauskas and C. Volpe, *Nucl. Phys. A* **792**, 219–228 (2007).

[66] W. Almosly, B. G. Carlsson, J. Dobaczewski, J. Suhonen, J. Toivanen, P. Vesely, and E. Ydrefors, *Phys. Rev. C* **89**, 024308 (2014).

[67] M.-K. Cheoun, E. Ha, T. Hayakawa, T. Kajino, and S. Chiba, *Phys. Rev. C* **82**, 035504 (2010).

[68] M.-K. Cheoun, E. Ha, K. S. Kim, and T. Kajino, *J. Phys. G: Nucl. Part. Phys.* **37**, 055101 (2010).

[69] M.-K. Cheoun, E. Ha, T. Hayakawa, S. Chiba, K. Nakamura, T. Kajino, and G. J. Mathews, *Phys. Rev. C* **85**, 065807 (2012).

[70] N. Paar, D. Vretenar, T. Marketin, and P. Ring, *Phys. Rev. C* **77**, 024608 (2008).

[71] H. Đapo and N. Paar, *Phys. Rev. C* **86**, 035804 (2012).

[72] E. Kolbe, K. Langanke, and G. Martinez-Pinedo, *Phys. Rev. C* **60**, 052801 (1999).

[73] E. Kolbe and K. Langanke, *Phys. Rev. C* **63**, 025802 (2001).

[74] T. Suzuki and M. Honma, *Phys. Rev. C* **87**, 014607 (2013).

[75] H. Hergert, J. M. Yao, T. D. Morris, N. M. Parzuchowski, S. K. Bogner, and J. Engel, *J. Phys.: Conf. Ser.* **0141**, 012007 (2018).

[76] J. Suhonen, *From Nucleons to Nucleus: Concepts of Microscopic Nuclear Theory* (Springer, Berlin, 2007).

[77] A. Bohr and B. R. Mottelson, *Nuclear Structure* (Benjamin, New York, 1969), Vol. 1.

[78] B. A. Brown, N. J. Stone, J. R. Stone, I. S. Towner, and M. Hjorth-Jensen, *Phys. Rev. C* **71**, 044317 (2005).

[79] M. Honma, T. Otsuka, T. Mizusaki, and M. Hjorth-Jensen, *Phys. Rev. C* **80**, 064323 (2009).

[80] J. Bardeen, L. N. Cooper, and J. R. Schrieffer, *Phys. Rev.* **108**, 1175 (1957).

[81] A. Bohr, B. R. Mottelson, and D. Pines, *Phys. Rev.* **110**, 936 (1958).

[82] A. H. Wapstra, G. Audi, *Nucl. Phys. A* **432**, 1–54 (1985).

[83] W. Almosly, E. Ydrefors, and J. Suhonen, *J. Phys. G: Nucl. Part. Phys.* **40**, 095201 (2013).

[84] P. Pirinen and J. Suhonen, *Phys. Rev. C* **91**, 054309 (2015).

[85] J. Suhonen and O. Civitarese, *Nucl. Phys. A* **924**, 1–23 (2014).

[86] O. Civitarese and J. Suhonen, *Phys. Rev. C* **89**, 044319 (2014).

[87] J. Toivanen and J. Suhonen, *Phys. Rev. C* **57**, 1237 (1998).

[88] J. Schwieger, A. Faessler, and T. S. Kosmas, *Phys. Rev. C* **56**, 2830 (1997).

[89] V. Tsakstara and T. S. Kosmas, *Phys. Rev. C* **83**, 054612 (2011).

[90] R. Foot and Z. K. Silagadze, *Acta Phys.Polon.* **B32**, 2271-2278 (2001), arXiv:astro-ph/0104251.

[91] A. Kashlinsky, *Astrophys. J. Lett.* **823**, L25 (2016).

[92] F. Kahlhoefer, *Int. J. Mod. Phys. A* **32**, 1730006 (2017).

[93] J. Conrad and O. Reimer, *Nature Physics* **13**, 224–231 (2017).

[94] D. Hooper and L. Goodenough, *Phys. Lett. B* **697**, 412–428 (2011).

[95] J. I. Read, *J. Phys. G: Nucl. Part. Phys.* **41**, 063101 (2014).

[96] F. J. Kerr, and D. Lynden-Bell, *Mon. Not. R. Astron. Soc.* **221**, 1023–1038 (1986).

[97] A. K. Drukier, K. Freese, and D. N. Spergel, *Phys. Rev. D* **33**, 3495–3508 (1986).

[98] P. J. McMillan, and J. J. Binney, *Mon. Not. R. Astron. Soc.* **402**, 934–940 (2010).

[99] M. J. Reid *et al.*, *Astrophys. J.* **700**, 137–148 (2009).

[100] T. Piffl *et al.*, *Astron. Astrophys.* **562**, A91 (2014).

[101] M. Farina, D. Pappadopulo, A. Strumia, and T. Volansky, *JCAP* **11**, 010 (2011).

[102] R. Catena, A. Ibarra, and S. Wild, *JCAP* **05**, 039 (2016).

[103] C. Tomei, on behalf of the SABRE collaboration, *Nuclear Instruments and Methods in Physics Research A* **845**, 418–420 (2017).

[104] P. C. Divari and J. D. Vergados, *Int. J. Mod. Phys. A* **29**, 1443003 (2014).

[105] B. A. Brown and W. D. M. Rae, *Nuclear Data Sheets* **120**, 115–118 (2014).

[106] B. Cheal *et al.*, *Phys. Rev. Lett.* **104**, 252502 (2010); B.A. Brown, and A.F. Lisetskiy, unpublished.

[107] D. Akimov *et al.*, *Science* **357**, 1123 (2017).

[108] T. S. Kosmas and J. D. Vergados, *Phys. Rev. D* **55**, 1752 (1997).

[109] J. D. Vergados and T. S. Kosmas, *Phys. Atom.Nucl.* **61**, 1066–1080 (1998).

[110] K. G. Savvidy and J. D. Vergados, *Phys. Rev. D* **87**, 075013 (2013).

[111] C. Alduino *et al.*, *Int. J. Mod. Phys. A* **33**, 1843002 (2018).

[112] J. H. Davis, *JCAP* **03**, 012 (2015) .

[113] J. B. Dent, B. Dutta, J. L. Newstead, and L. E. Strigari, *Phys. Rev. D* **93**, 075018 (2016).

[114] J. B. Dent, B. Dutta, J. L. Newstead, and L. E. Strigari, *Phys. Rev. D* **95**, 051701(R) (2017).

[115] C. A. J. O'Hare, A. M. Green, J. Billard, E. Figueroa-Feliciano, and L. E. Strigari, *Phys. Rev. D* **92**, 063518 (2015).

[116] P. Grothaus and M. Fairbairn, *Phys. Rev. D* **90**, 055018 (2014).

[117] G. Battistoni, A. Ferrari, T. Montaruli, and P. R. Sala *Astropart. Phys.* **23**, 526–534 (2005).

[118] C. Lunardini, *Astropart. Phys.* **26**, 190–201 (2006).

[119] Solar neutrino data http://www.sns.ias.edu/∼jnb/SNdata/sndata.html.

[120] J. N. Bahcall, A. M. Serenelli, and S. Basu, *Astrophys. J.* **621**, L85–L88 (2005).

[121] H. T. Janka and W. Hillebrandt, *Astron. Astrophys.* **224**, 49–56 (1989).

[122] M. T. Keil, G. G. Raffelt, and H.-T. Janka, *Astrophys. J.* **590**, 971–991 (2003).

[123] H. Duan and J. P. Kneller, *J. Phys. G: Nucl. Part. Phys.* **36**, 113201 (2009).

[124] J. Gava and C. Volpe, *Phys. Rev. D* **78**, 083007 (2008).

[125] A. B. Balantekin and G. M. Fuller, *Phys. Lett. B* **471**, 195–201 (1999).

[126] G. G. Raffelt, *Prog. Part. Nucl. Phys.* **64**, 393–399 (2010).

[127] G. Martínez-Pinedo, B. Ziebarth, T. Fischer, and K. Langanke, *Eur. Phys. J. A* **47**, 98 (2011).

[128] K. Nakamura and Particle Data Group, *J. Phys. G: Nucl. Part. Phys.* **37**, 075021 (2010).

[129] E. Kolbe, K. Langanke, G. Martínez-Pinedo, and P. Vogel, *J. Phys. G: Nucl. Part. Phys.* **29**, 2569 (2003).

[130] J. Engel, *Phys. Rev. C* **57**, 2004 (1998)

[131] J. D. Walecka, *Theoretical Nuclear and Subnuclear Physics* (Imperial College Press, London, 2004).

[132] J. S. O'Connell, T. W. Donnelly, and J. D. Walecka, *Phys. Rev. C* **6**, 719 (1972).

[133] J. N. Bahcall, E. Lisi, D. E. Alburger, L. De Braeckeleer, S. J. Freedman, and J. Napolitano, *Phys. Rev. C* **54**, 411 (1996).

[134] Z. M. Niu, Y. F. Niu, H. Z. Liang, W. H. Long, and J. Meng, *Phys. Rev. C* **95**, 044301 (2017).

[135] Y.-Z. Qian, W. C. Haxton, K. Langanke, and P. Vogel, *Phys. Rev. C* **55**, 1532 (1997).